



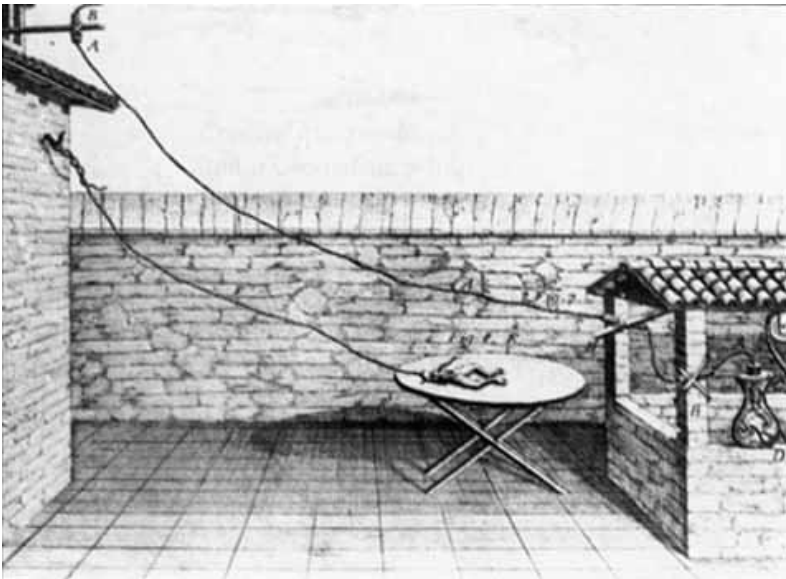
Sainsbury Wellcome Centre

Feb. 6, 2018

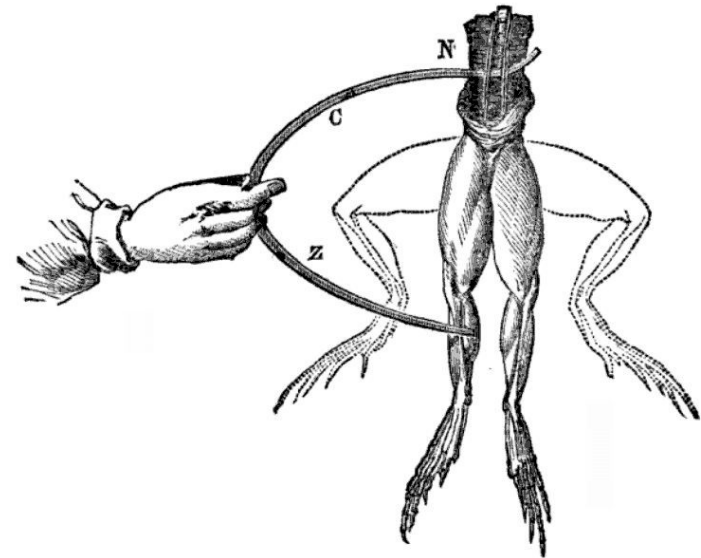
Methods for recording neuronal activity

Prof. Tom Otis
t.otis@ucl.ac.uk

From 'animal electricity'... to how nerves work



Galvani, 1780



Galvani, 1791

First electrical recordings of a nerve impulse

frog sciatic nerve

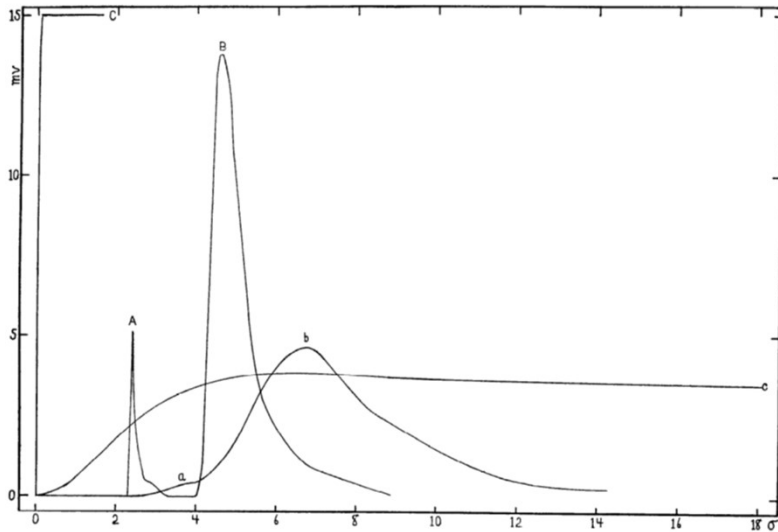


Fig. 3. The action currents of the bull frog sciatic, as recorded by the Braun tube and string galvanometer, plotted in rectangular linear coördinates. *A, B, C*, Braun tube records; *a, b, c*, string galvanometer records. *A, a*, shock; *B, b*, action current; *C*, calibration with a constant current of 15 mv.; *c*, with one of 3.75 mv.



Herbert Gasser



Joseph Erlanger

American J. Physiol., 1922



Herbert Spencer Gasser

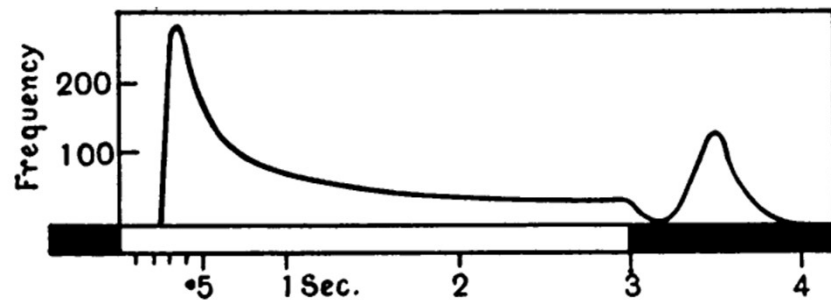
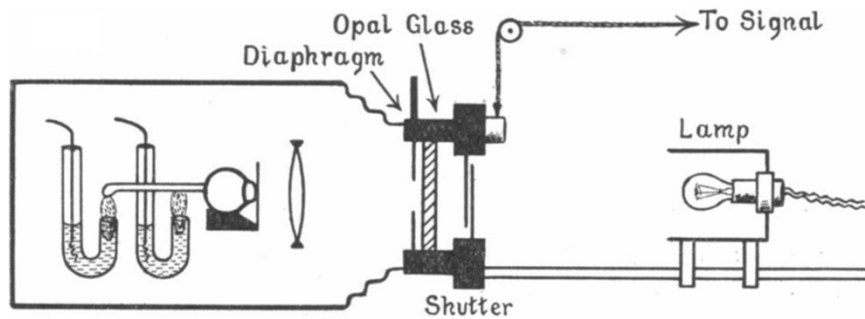
Rockefeller Institute for Medical Research, New York
neurophysiology

	All	Since 2013
Citations	7692	406
h-index	39	10
i10-index	57	11

TITLE	CITED BY	YEAR
Electrical signs of nervous activity J Erlanger, HS Gasser	957	1937
Axon diameters in relation to the spike dimensions and the conduction velocity in mammalian A fibers HS Gasser, H Grundfest American Journal of Physiology--Legacy Content 127, 393-414	553	1939
The dynamics of muscular contraction HS Gasser, AV Hill Proceedings of the Royal Society of London. Series B, containing papers of a ...	535	1924
The role of fiber size in the establishment of a nerve block by pressure or cocaine HS Gasser, J Erlanger American Journal of Physiology--Legacy Content 88, 581-591	464	1929
The role played by the sizes of the constituent fibers of a nerve trunk in determining the form of its action potential wave HS Gasser, J Erlanger American Journal of Physiology--Legacy Content 80, 522-547	403	1927
Properties of dorsal root unmyelinated fibers on the two sides of the ganglion HS Gasser The Journal of general physiology 38 (5), 709-728	369	1955
Potentials produced in the spinal cord by stimulation of dorsal roots. HS Gasser, HT Graham	339	1933

First recordings of light-evoked activity in optic nerve

Conger eel optic nerve



J. Physiology, 1927

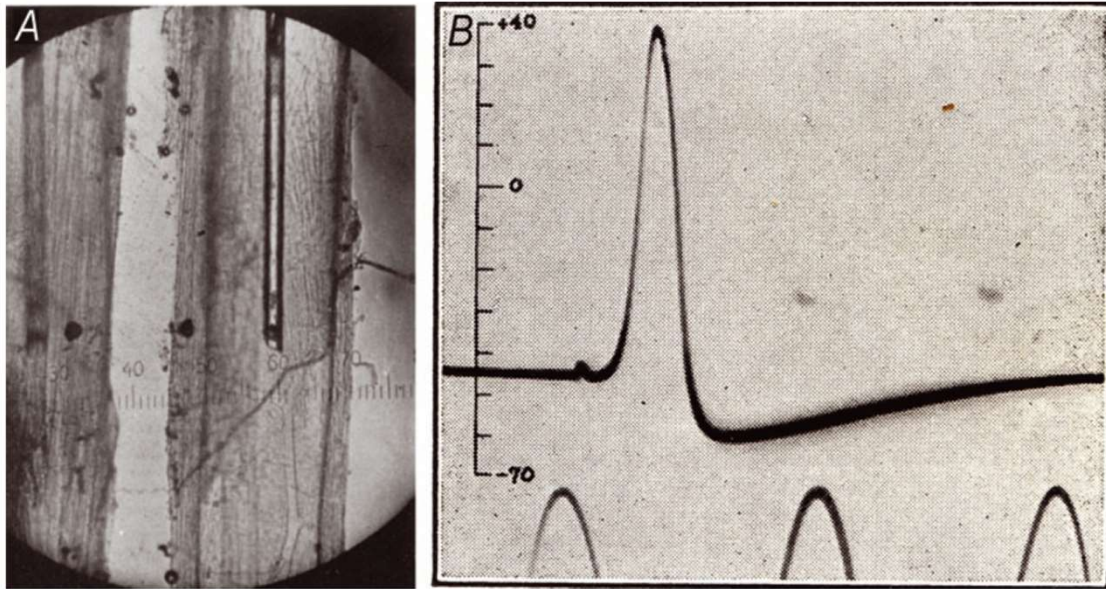


Lord Edgar Douglas
Adrian

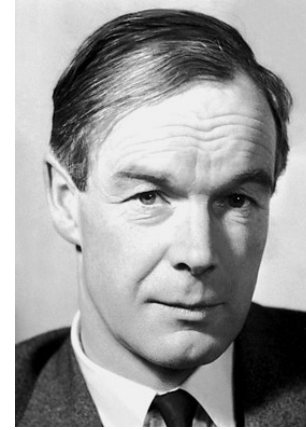
"I had arranged electrodes on the optic nerve of a toad in connection with some experiments on the retina. The room was nearly dark and I was puzzled to hear repeated noises in the loudspeaker attached to the amplifier, noises indicating that a great deal of impulse activity was going on. It was not until I compared the noises with my own movements around the room that I realised I was in the field of vision of the toad's eye and that it was signalling what I was doing."

Mechanism of the nerve impulse

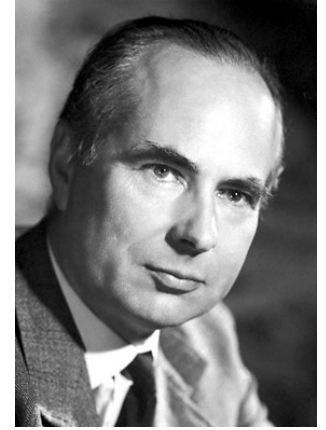
Squid giant axon



Nature, 1939



Alan Hodgkin



Andrew Huxley

Hodgkin Huxley model of the action potential

<http://nerve.bsd.uchicago.edu/>

Fig.1

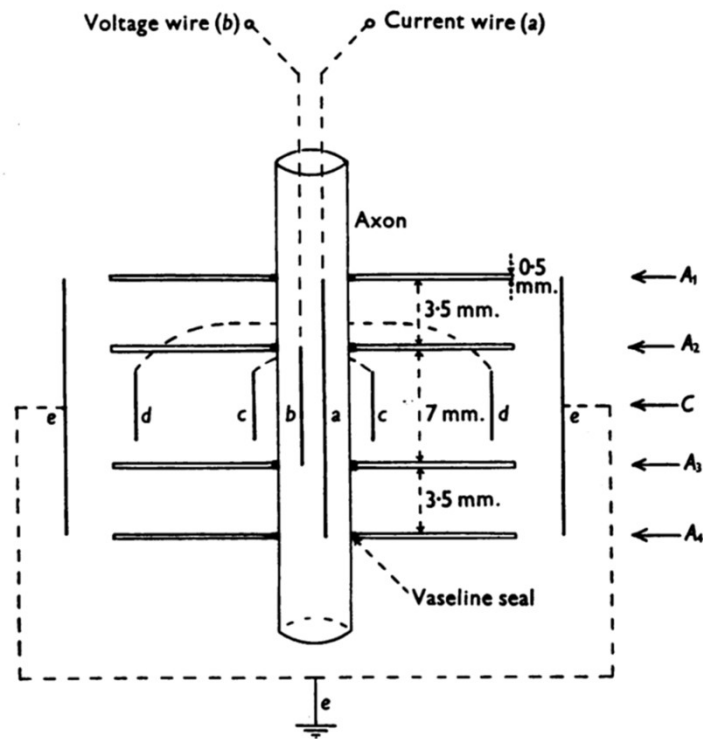
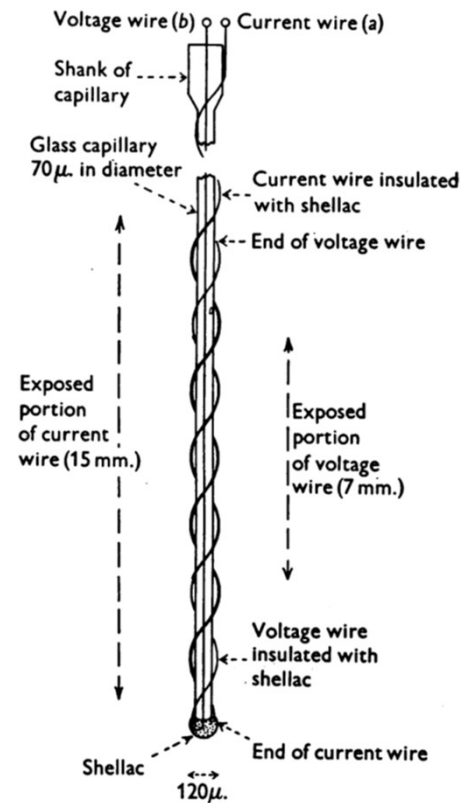


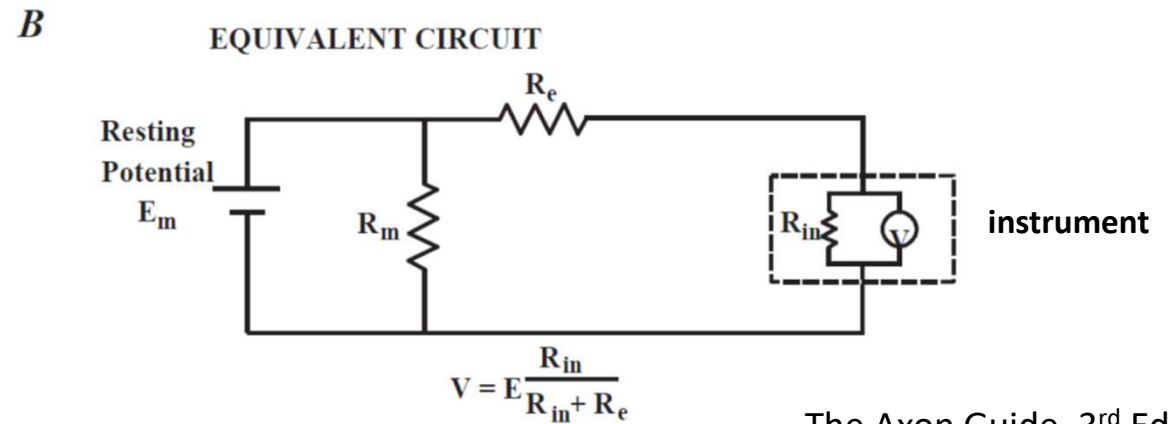
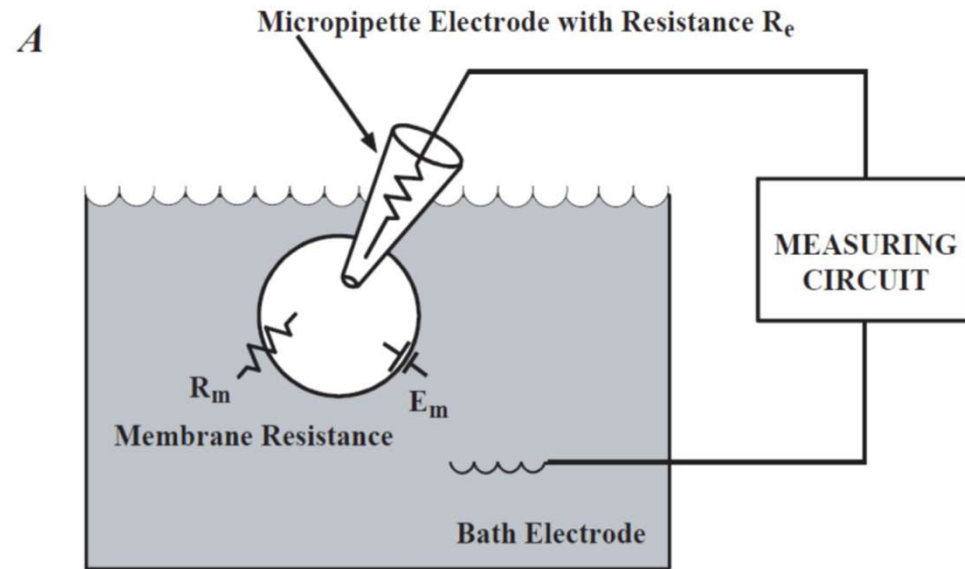
Fig.4



Hodgkin, Huxley, and Katz, J. Physiol., 1952

Intracellular measurements with a microelectrode

Ag/AgCl wires are standard in physiological contexts due to their excellent bidirectional ionic mobility, stability



The Axon Guide, 3rd Ed.

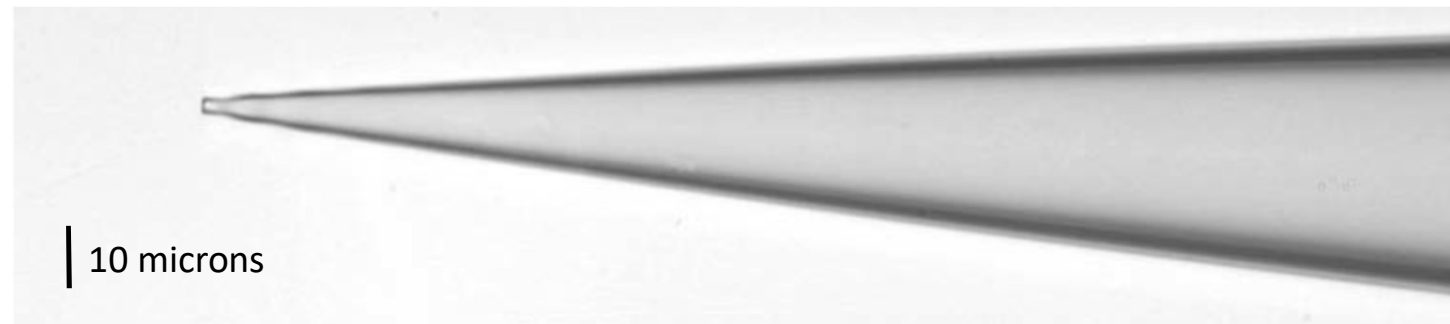
Microelectrode methods for intracellular recording

'sharp' microelectrode



3 M KCl, 3 M K Acetate
80-100 M Ω

whole-cell patch pipette



physiological internal
e.g. 130 K MeSO₄
2-5 M Ω

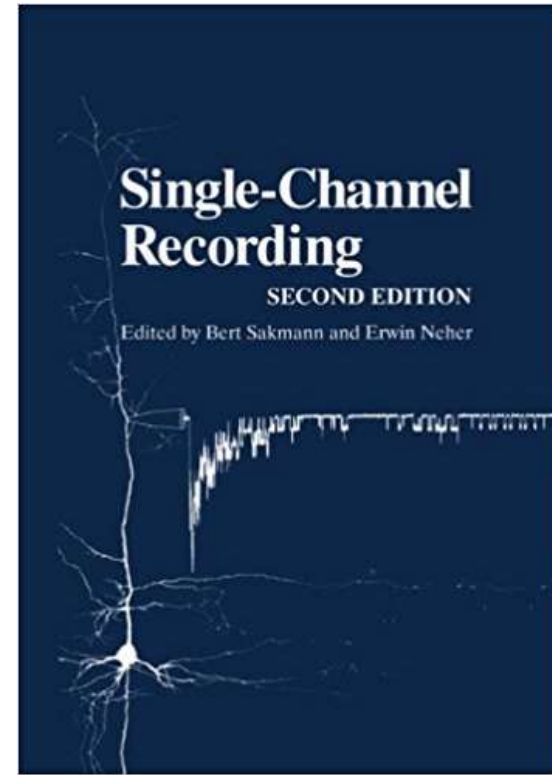
Patch clamping



Bert Sakmann



Erwin Neher



<https://youtu.be/M3xN4lhmt7U>

from Purves et al, Neuroscience 5th Ed. 2012

Microelectrode methods for intracellular recording

Rat dentate gyrus granule cells

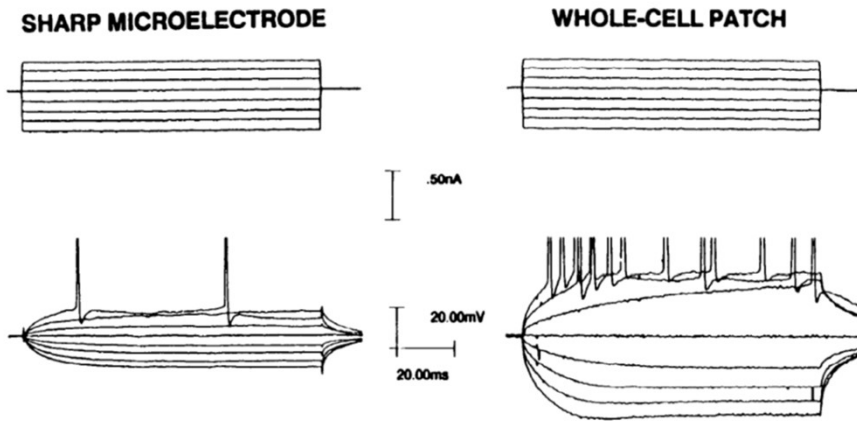


FIG. 4. Comparison of membrane voltage responses to current steps in GCs recorded with sharp electrode vs. whole-cell patch electrode. Sharp electrode filled with 3 M potassium acetate. The differences in R_N and τ_m can be appreciated by visual inspection of the records. Spike threshold is similar for the 2 recording methods.

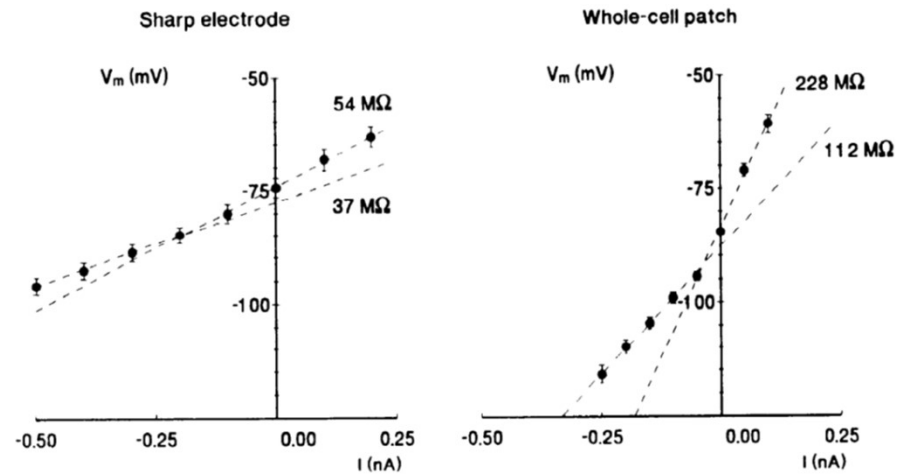
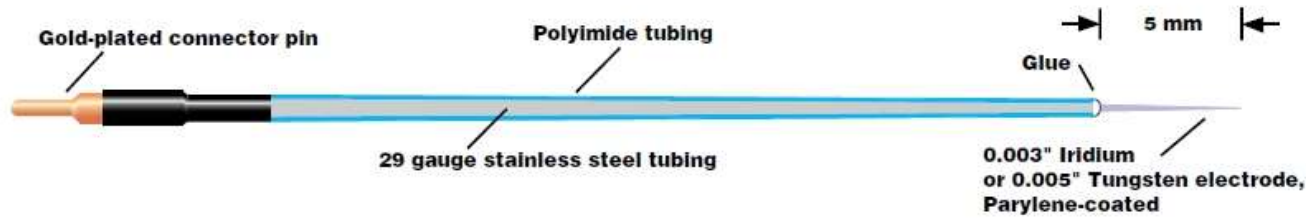


FIG. 5. Membrane voltage vs. injected current for 31 GCs recorded in whole-cell method and 10 GCs recorded with sharp electrodes; points are means \pm SE. Voltage was determined 180 ms after start of current pulse. Error bars indicate SE. Lines are fitted by least-squares method. Regions of linearity determined by eye.

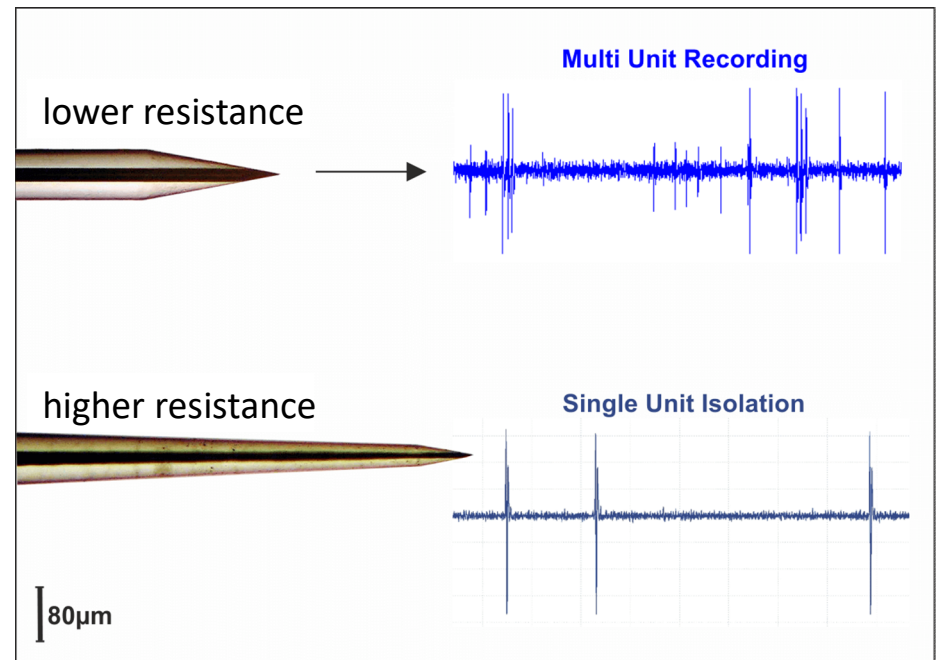
Staley et al., *J. Neurophysiol.* **67**: 1346, 1992

Metal electrodes



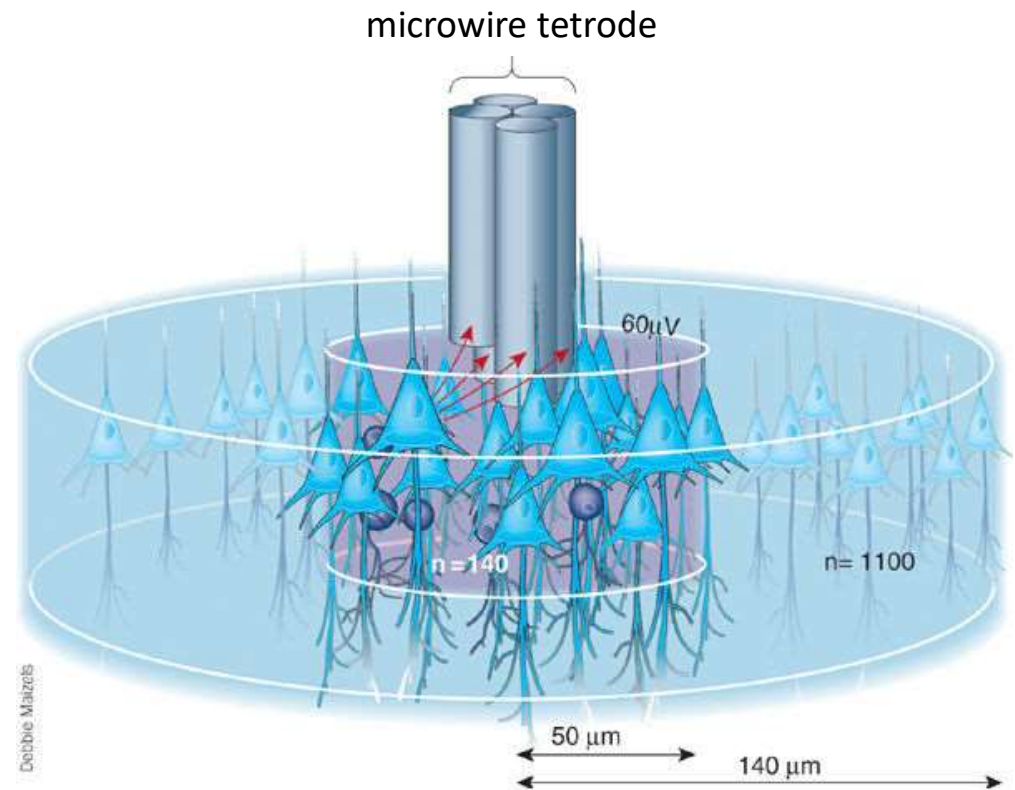
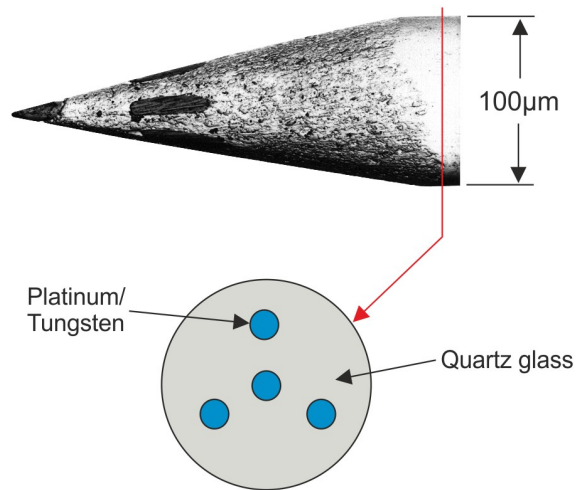
tungsten
iridium
platinum/iridium

glass-coated
polyimide-coated



Recording from populations of single neurons: tetrodes

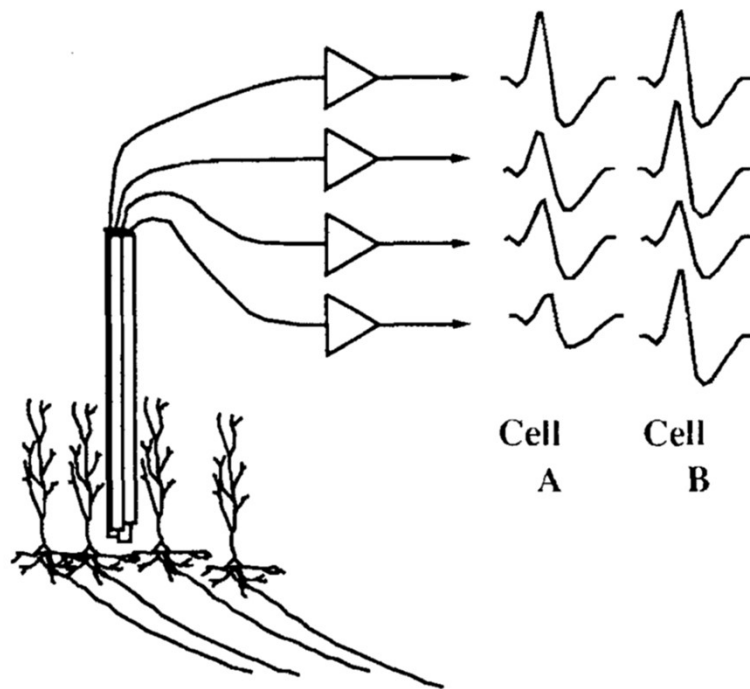
Thomas Recording tetrode



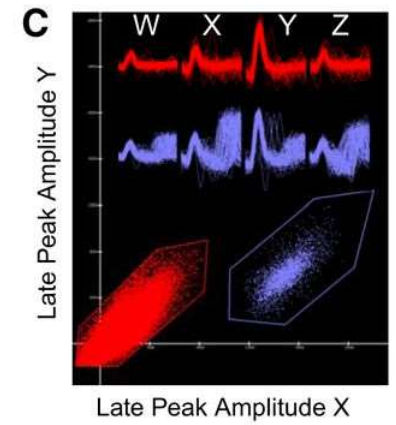
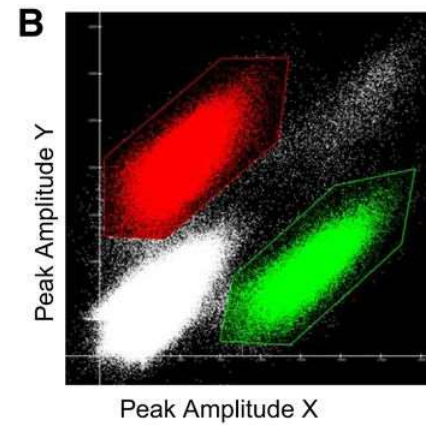
see Recce & O'Keefe, 1989

Buzsáki, *Nat. Neurosci.* 2004

Recording from populations of single neurons: tetrodes

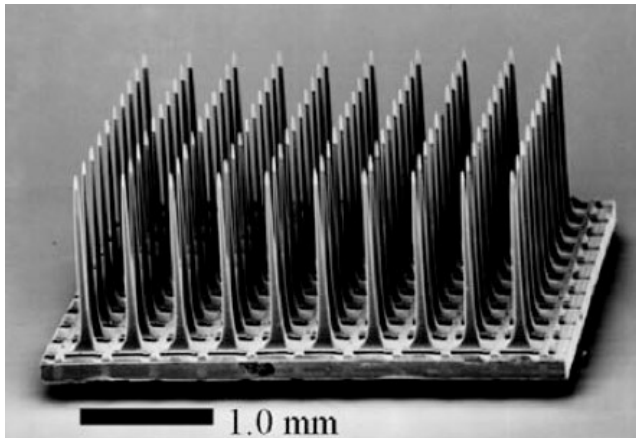


O'Keefe & Recce, 1993

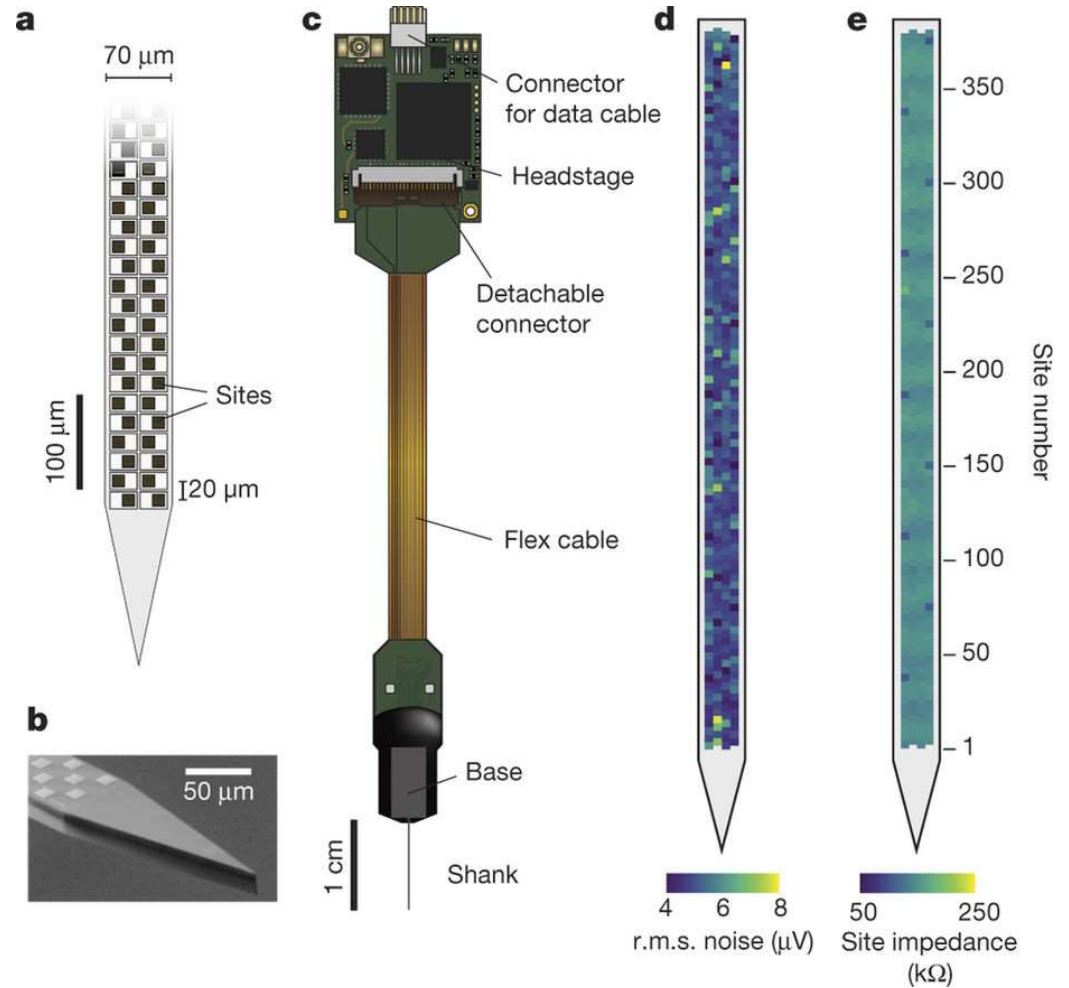


Halverson et al., J. Neurosci. 35:7182-32, 2015

Utah array to Neuropixel probes



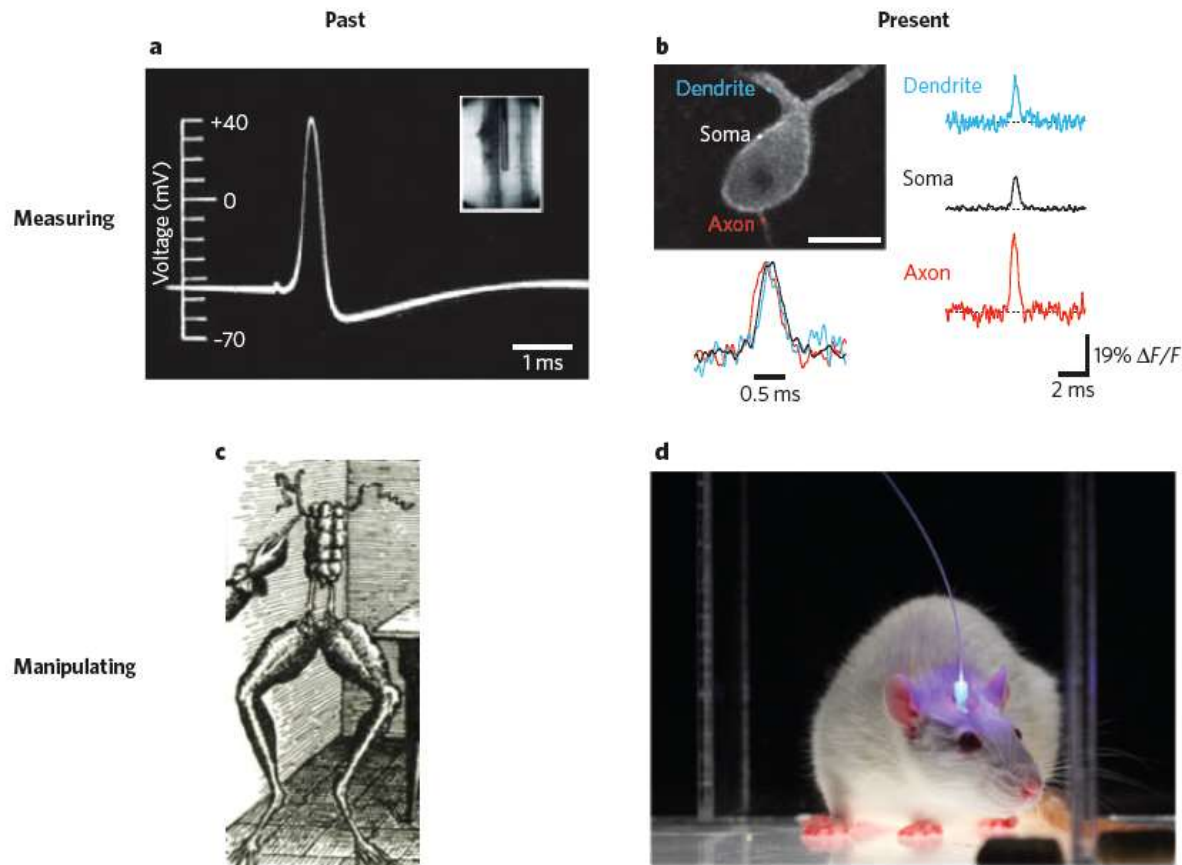
R. Normann, Uni. Utah
see also <https://www.youtube.com/watch?v=ItI6PqSTdHQ>
& Kelly et al, *J. Neurosci.* **27**:261-74, 2007



Jun et al., *Nature* 2017

Electrophysiology in the age of light

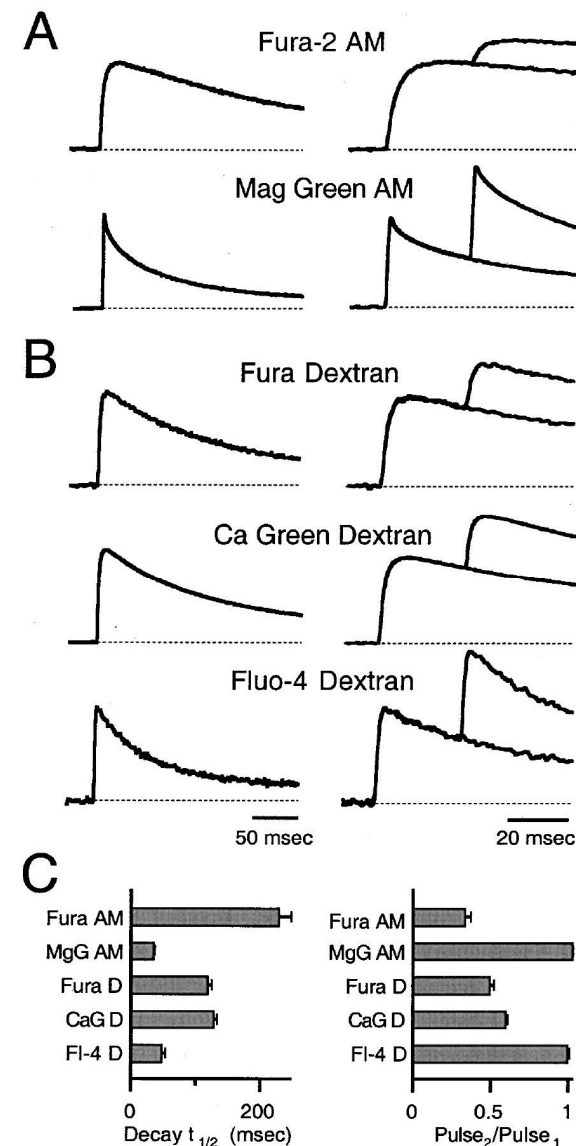
Massimo Scanziani¹ & Michael Häusser²



Small molecule Ca^{++} dyes: A range of affinities and kinetics

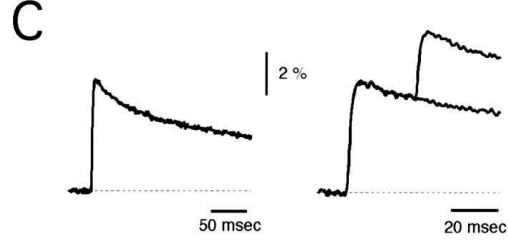
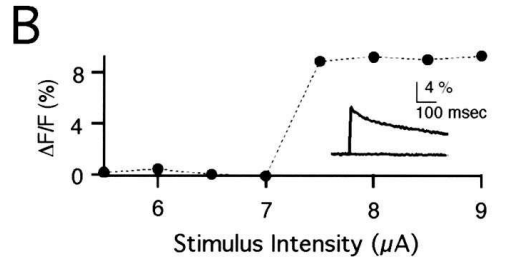
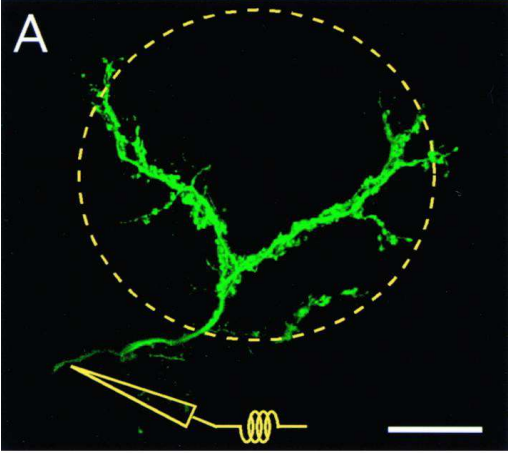
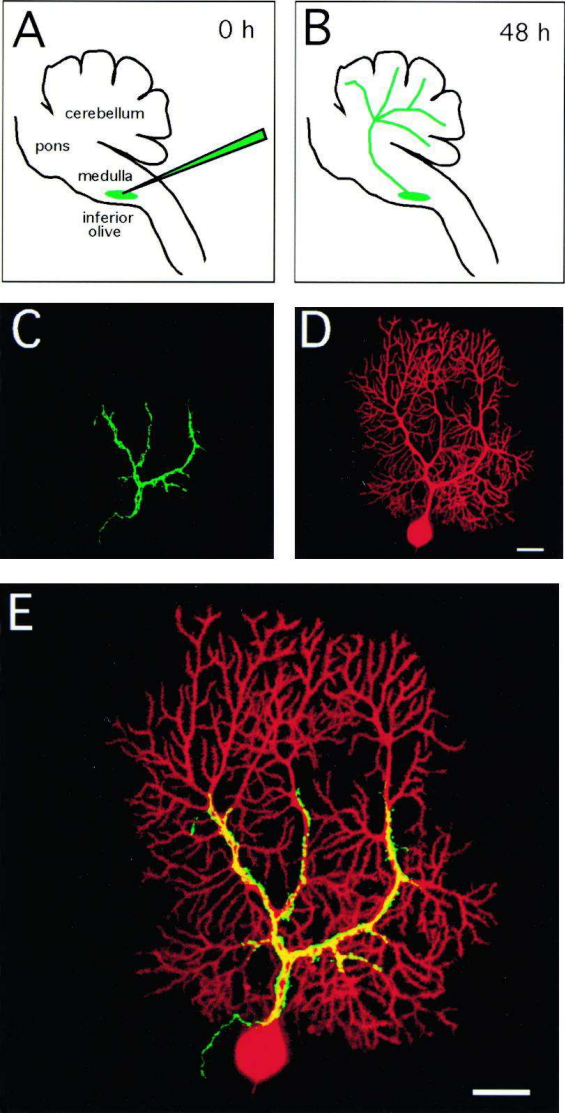
Table 1. SM Dye Dissociation Constants for Calcium

Small Molecule dye	K_D (μM)	Reference
Fura-2	0.16	(Kao and Tsien 1988)
Magnesium green	7	(Zhao et al. 1996)
Fura dextran (10,000 MW)	0.52	(Konishi and Watanabe 1995)
Calcium green dextran (3,000 MW)	0.54	(Haugland 1996)
Fluo-4 dextran (10,000 MW)	3.1	



Kreitzer et al., *Neuron* 27:25 (2000)

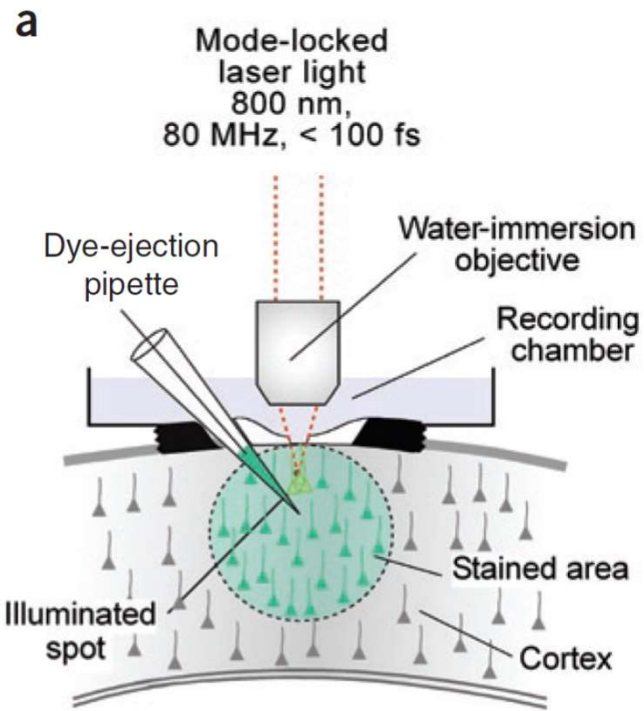
Dye imaging from a presynaptic terminal



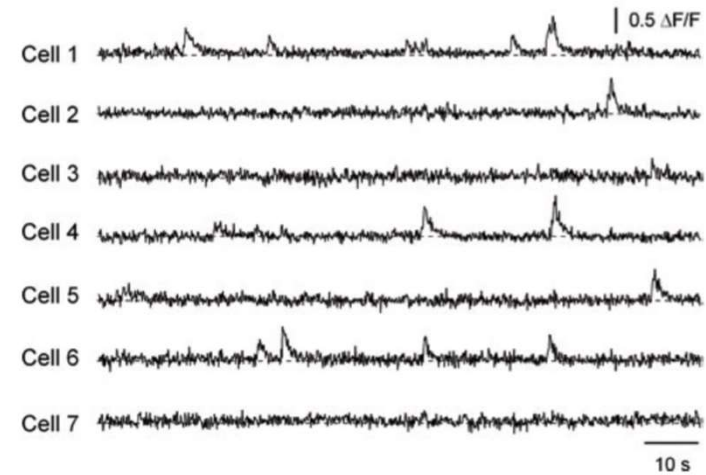
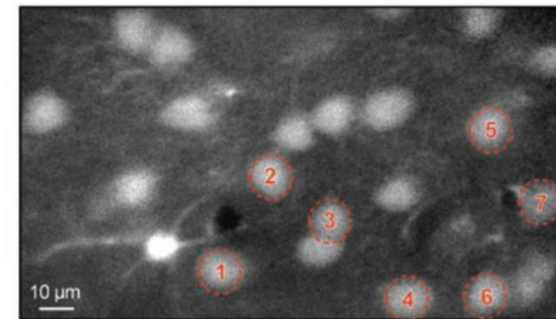
Kretzner et al., *Neuron* 27:25 (2000)

Ca⁺⁺ dyes *in vivo*

'Bulk loading'

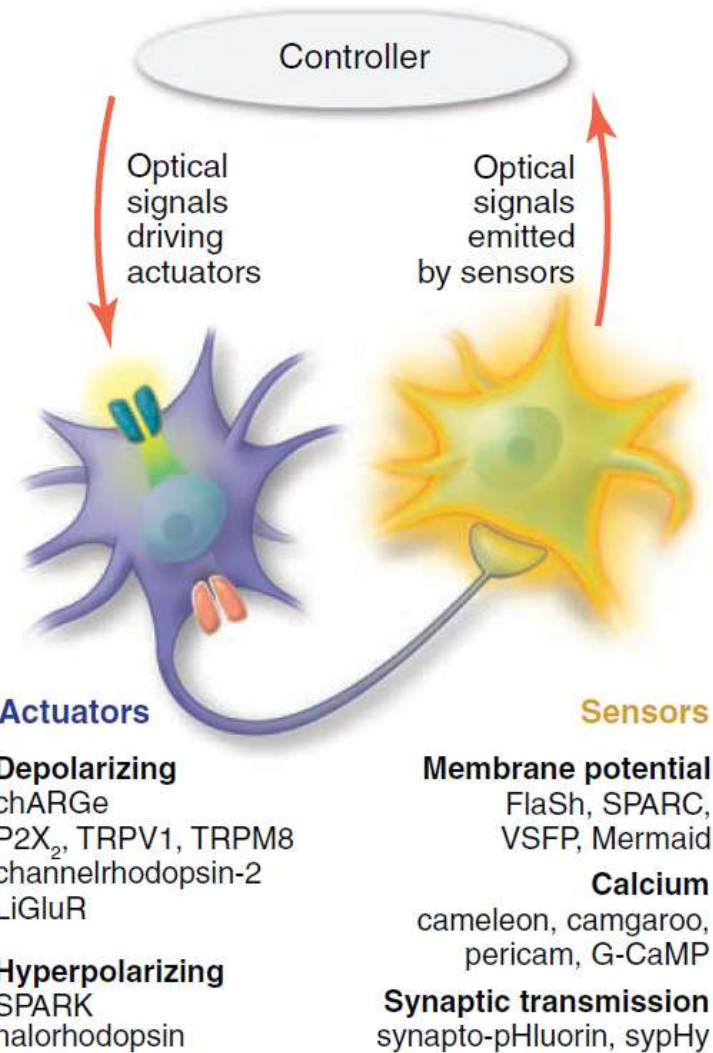


Adult (6-month-old)



Garaschuk & Konnerth, *Nature Protocols* 1:380-6, 2006

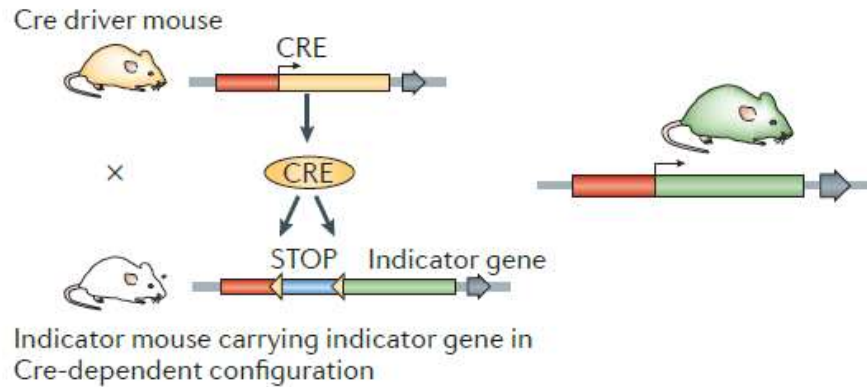
Optogenetic *sensors* and *actuators*



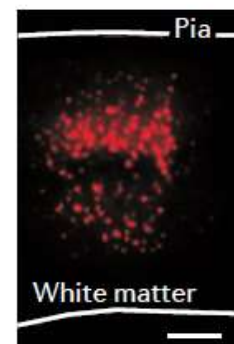
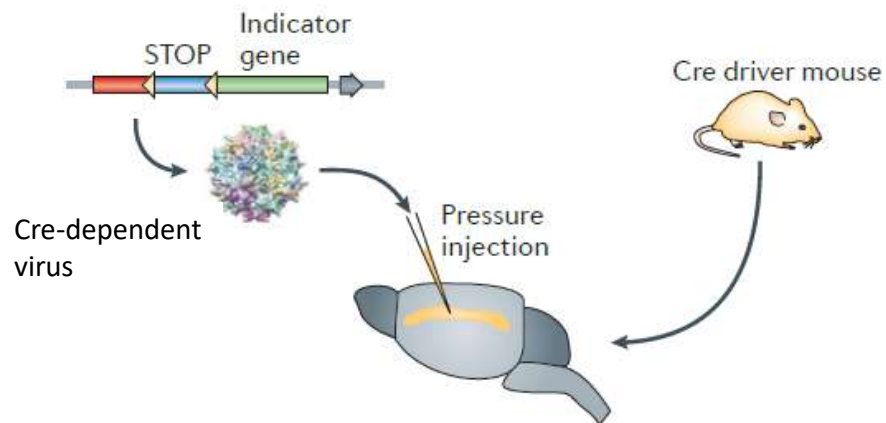
Miesenböck, *Science*, 2009

Conditional genetics and lab mice

Breeding strategy



Viral strategy

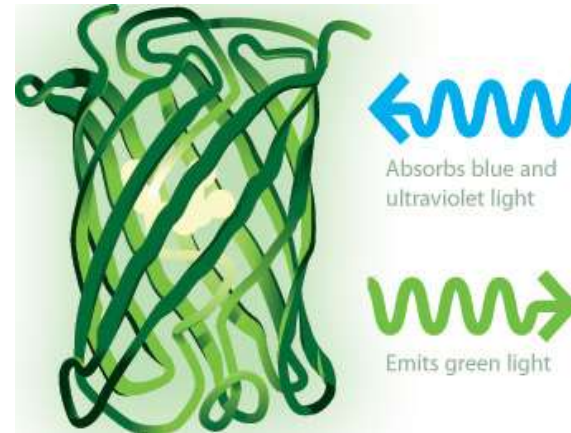


from Knopfel,
Nat. Rev. Neurosci.
2012

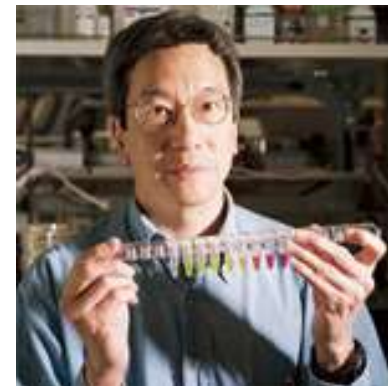
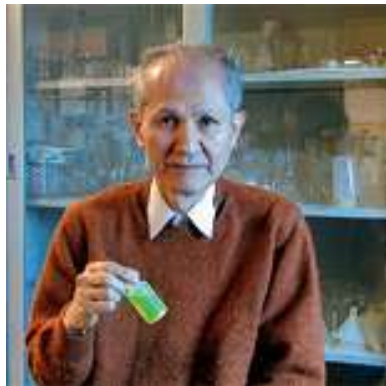
A revolution in biotechnology caused by a protein from a jellyfish



Green fluorescent protein



2008 Nobel prize in Chemistry: Shimomura, Chalfie, & Tsien



Fundamentals of fluorescence

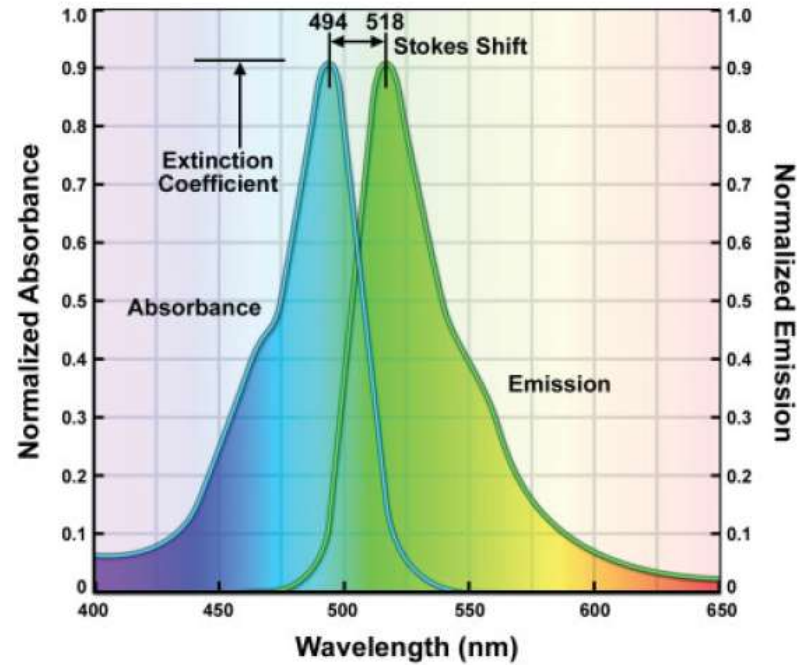


Figure 11.3

Normalized absorption and fluorescence emission spectra of fluorescein conjugated to IgG. Both spectra span a wide range of wavelengths. Fluorescein has an absorption/excitation peak at 494 nm and looks yellow-green to the eye, but actually fluoresces at wavelengths ranging from blue to red with a peak at 518 nm. The difference in nanometers between the excitation and emission maxima is called the Stokes shift. The molar extinction coefficient is measured at the peak of the absorbance spectrum as indicated in the figure.

Multicolored fluorescent proteins

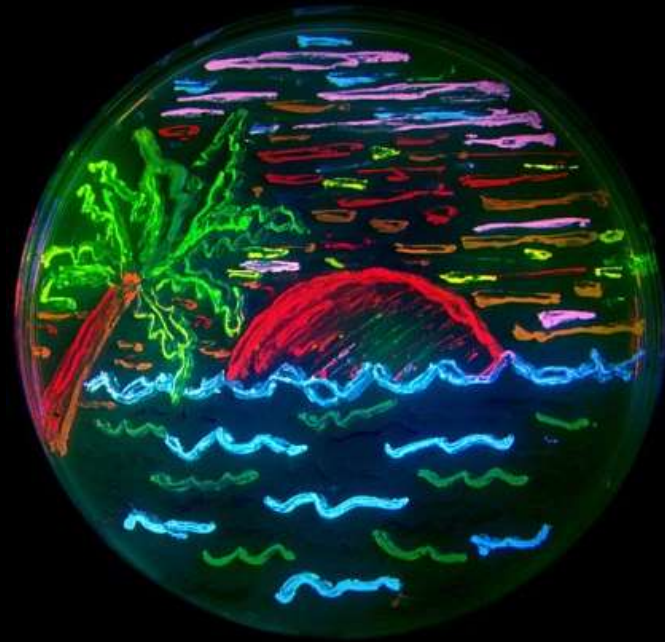


TABLE 11.2 Physical Properties of Useful Fluorescent Proteins

Protein ^a	Color ^b	Excitation (nm)	Emission (nm)	Brightness ^c	Photostability ^d	Filter Set ^e
EBFP2	Blue	383	448	18	++	DAPI
mCerulean	Cyan	433	475	17	++	CFP
mTurquoise	Cyan	433	474	25	+++	CFP
mTFP1	Teal	462	492	54	+++	CFP
mEGFP	Green	488	507	34	++++	FITC/GFP
mEmerald	Green	487	509	39	++++	FITC/GFP
mVenus	Yellow	515	528	53	++	FITC/YFP
mCitrine	Yellow	516	529	59	++	FITC/YFP
mKO2	Orange	551	565	40	+++	TRITC
tdTomato	Orange	554	581	95	+++	TRITC
TagRFP	Orange	555	584	48	++	TRITC
mApple	Orange	568	592	37	+++	TRITC
mCherry	Red	587	610	17	+++	TxRed
mKate2	Far-Red	588	633	25	++	TxRed
mPlum	Far-Red	590	649	3.2	+++	TxRed
mNeptune	Far-Red	600	650	13	++++	Cy5

^a Common literature abbreviation.

^b Spectral class.

^c Product of the molar extinction coefficient and the quantum yield ($\text{mM} \times \text{cm}^{-3}$).

^d Relative to mEGFP (++++).

^e Recommended filter set.

From Murphy and Davidson, Ch 11

Circularly-permuted GFP and 'CAMgaroo'

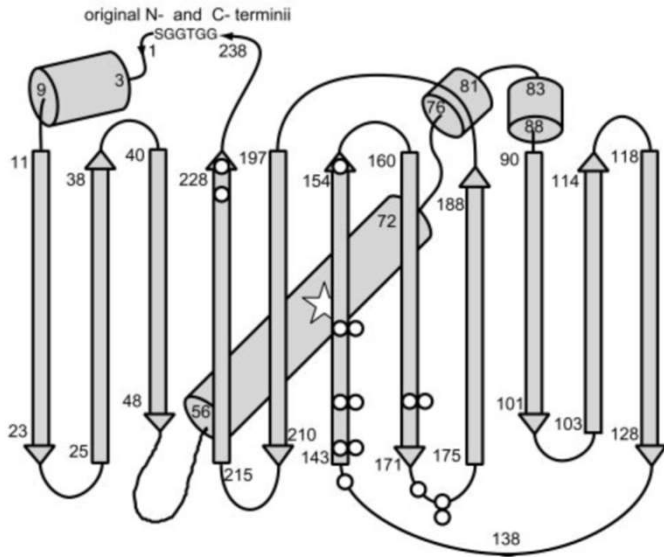


FIG. 2. Schematic drawing of the overall fold of GFP (12) modified to show starting points of fluorescent circular permutations (○), the linker (GGTGGS) connecting the original N and C termini, and the approximate location of the chromophore (open star, residues 65–67). Locations with two circles indicate where circular permutations with two different ending amino acids were isolated (Table 1).

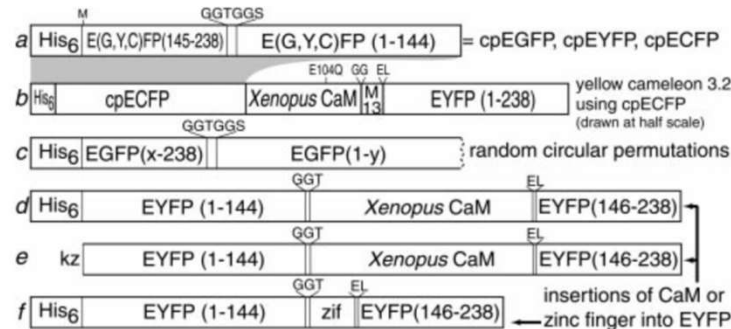
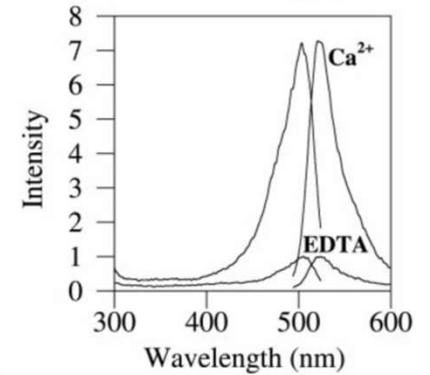


FIG. 1. Schematic structures of major new constructs. (a) Designed circular permutations of EGFP, EYFP, and ECFP starting at Y145M. His₆ indicates the polyhistidine tag MRGSHHHHHGMASMTG-GQQMGRDLYDDDDDKDP. Linkers and substitutions are shown above the main sequence. (b) Yellow cameleon 3.2 (YC3.2) incorporating cpECFP instead of ECFP. This sequence is drawn at half the scale of all the other constructs. M13 is the CaM-binding peptide derived from skeletal muscle myosin light chain kinase (7). (c) Random circular permutations of EGFP. The successful values of x and y are shown in Table 1. (d and e) Insertions of CaM in place of Y145 of EYFP as expressed in bacteria (d) for *in vitro* purification or in HeLa cells (e) for *in situ* monitoring of cytosolic Ca²⁺. kz, Kozak sequence (10) for optimal translation initiation. (f) Insertion of a zinc finger (zif), residues 334–362 of zif268 (8), in place of Y145 of EYFP.



An apt nickname for this construct is “camgaroo1,” because it is yellowish, carries a smaller companion (calmodulin) inserted in its “pouch,” can bounce high in signal, and may spawn improved progeny.

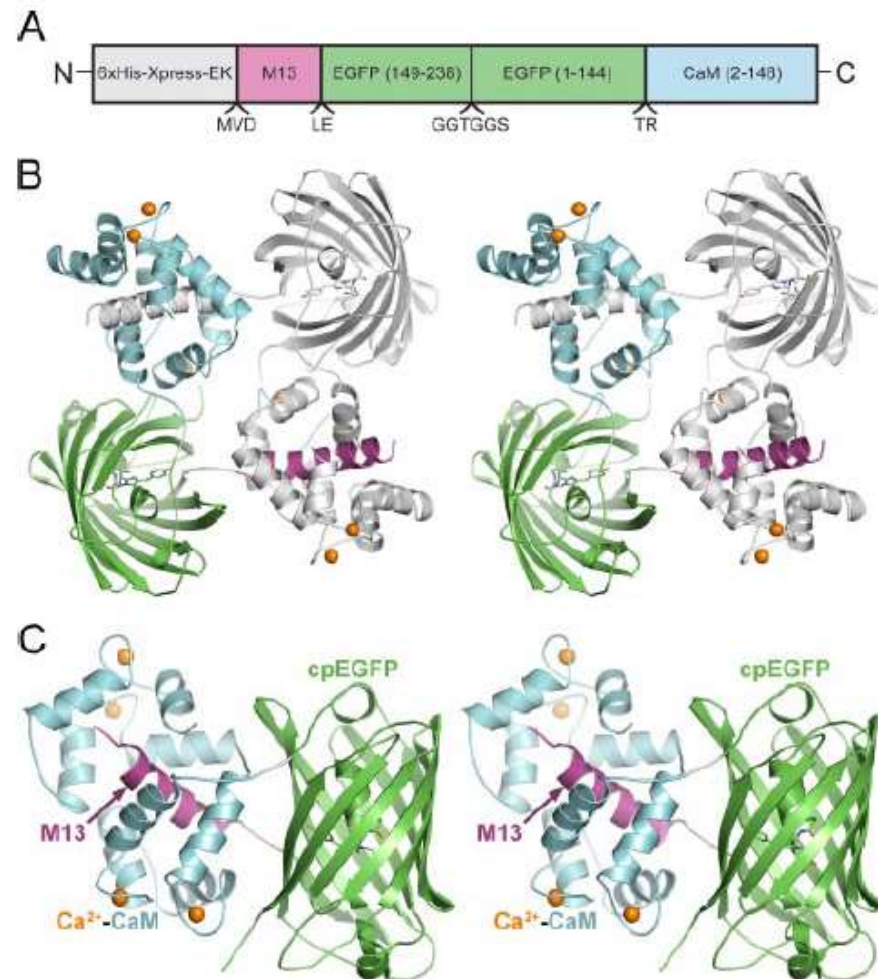
The GCaMP family of calcium sensors

GCaMP1 described in 2001:
Nakai et al., *Nat. Biotech.* 19:137

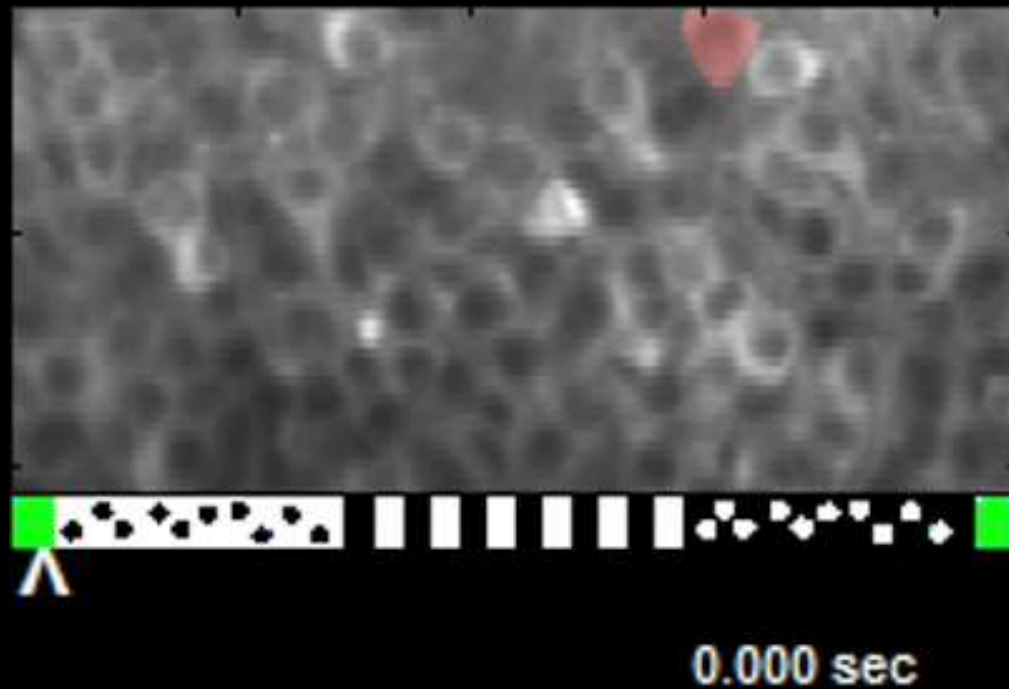
GCaMP6:
Chen et al., 2013
Nature, 499:295

See also **B-GECO** and
R-GECO

crystal structure of GCaMP2:
Akerboom et al., *JBC* 284:6455, 2009

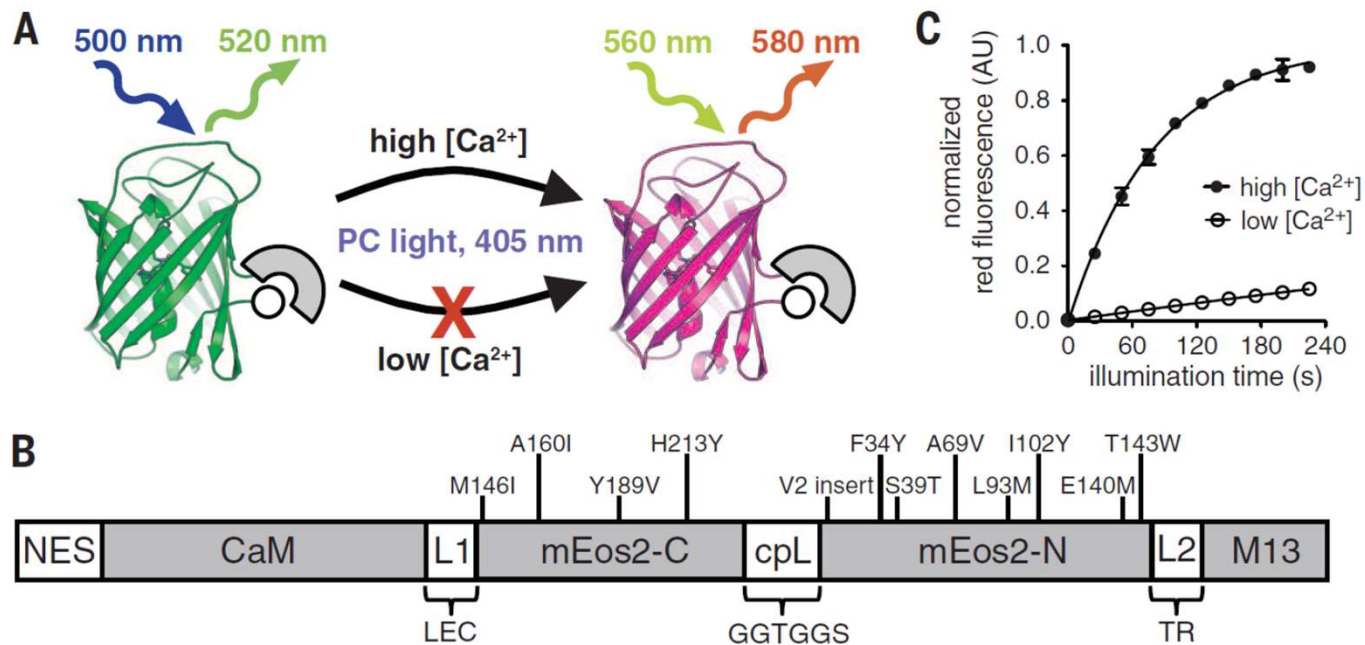


Imaging while the mouse navigates a virtual reality maze

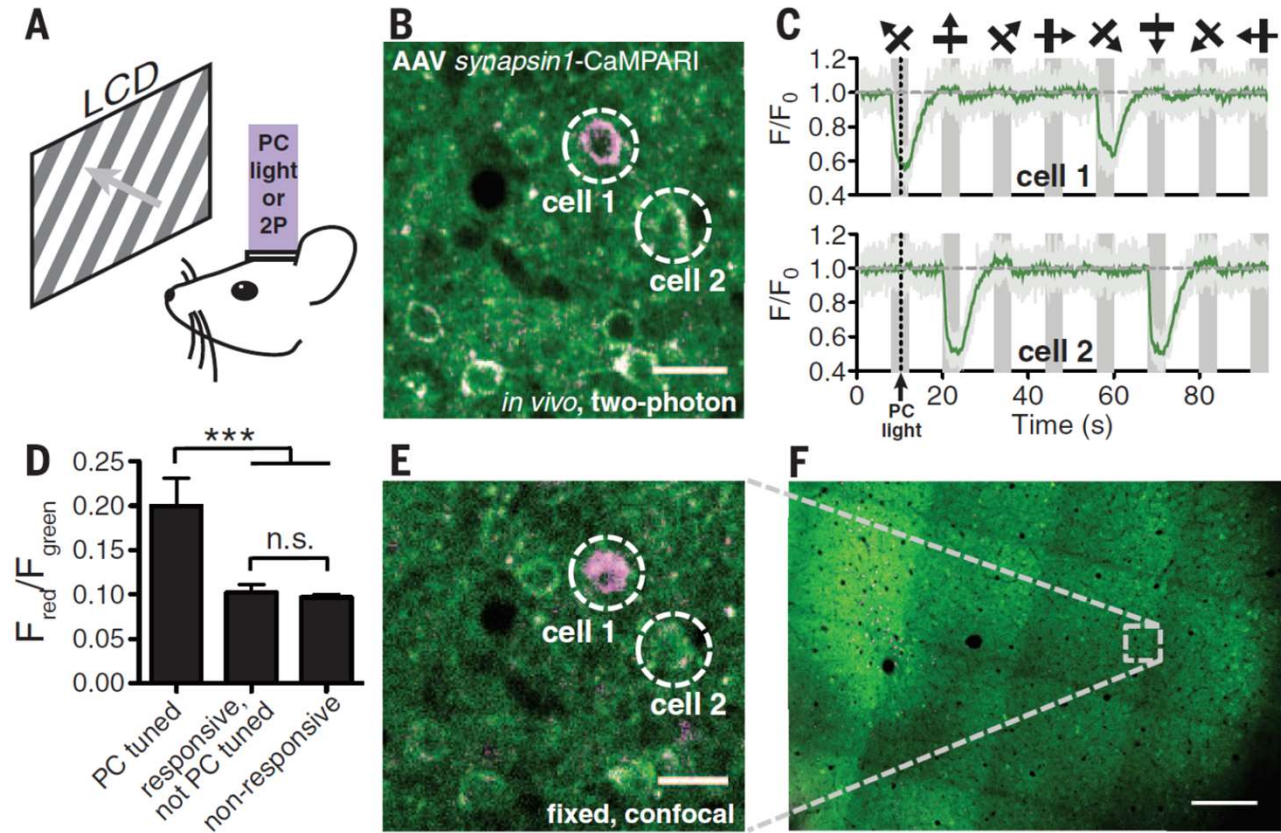


Dombeck et al., *Nature Neuroscience* 13:1433

CAMPARI, a conditional integrator of neural activity

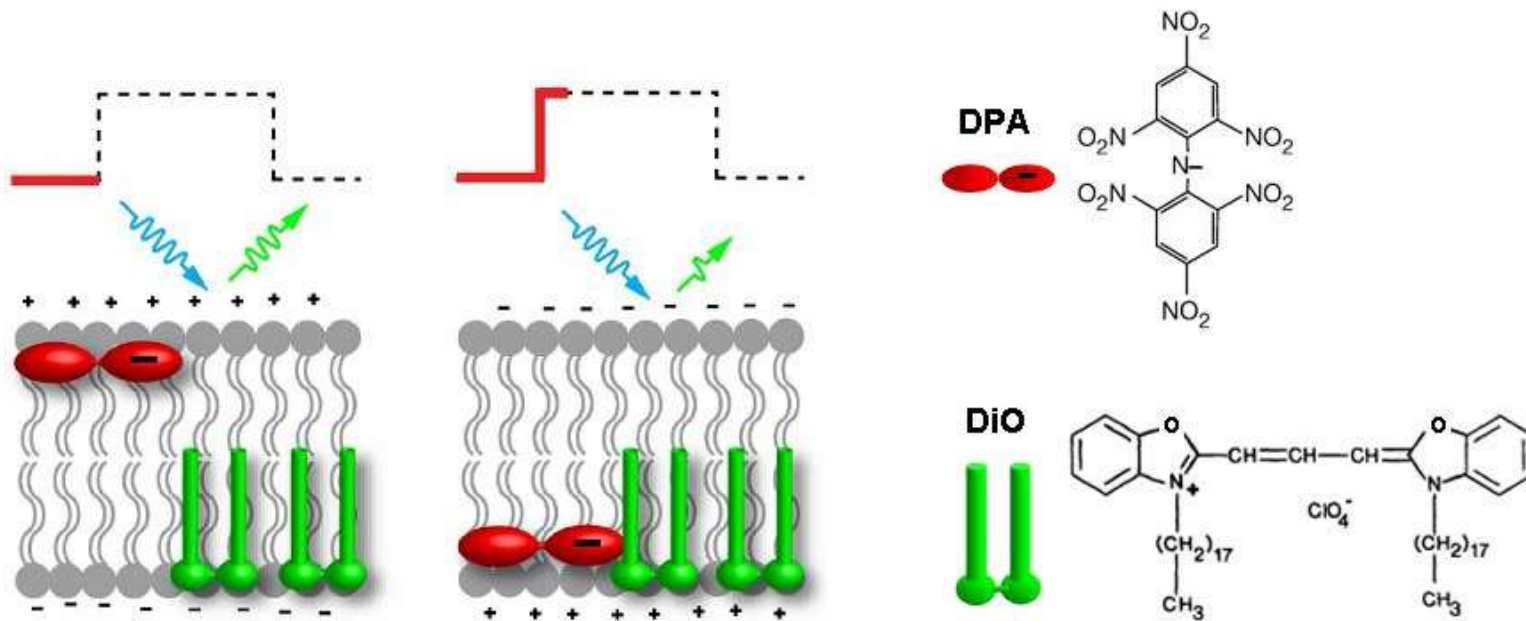


CAMPARI performance *in vivo*



Optical sensors of voltage

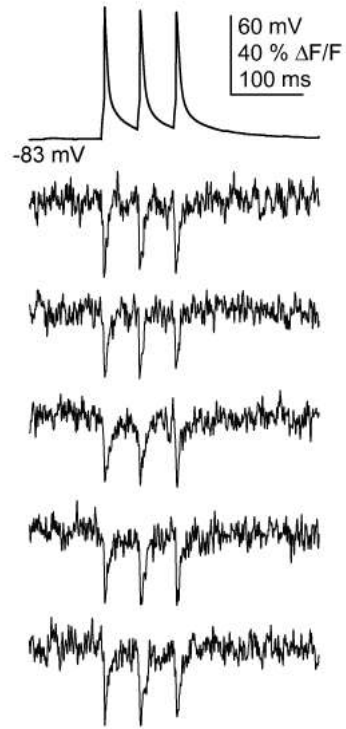
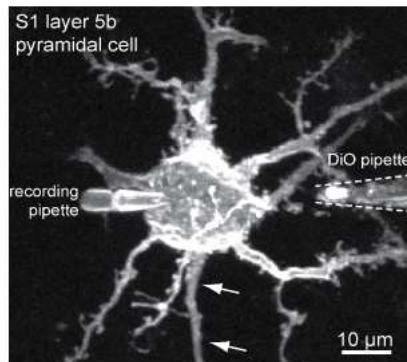
A non-genetic voltage sensor that relies on FRET-based quenching



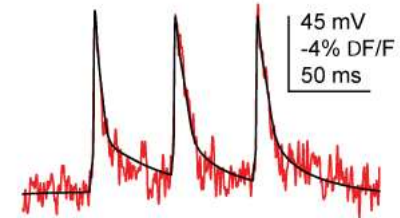
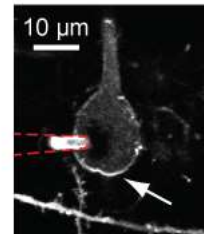
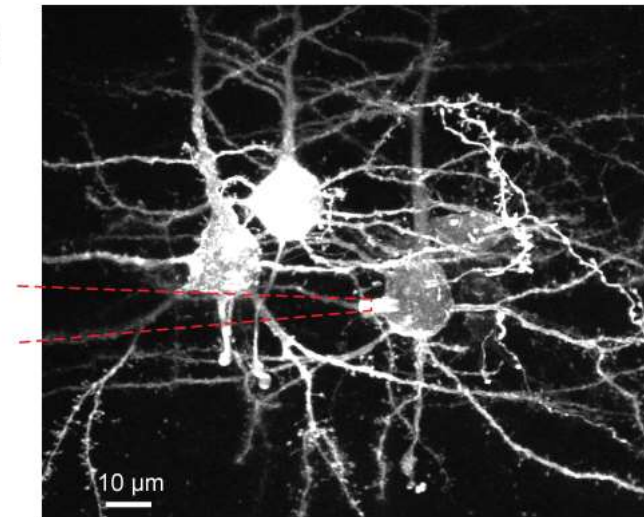
Bradley et al., *J. Neurosci.*, 2009

Two photon compatibility, high SNR

A



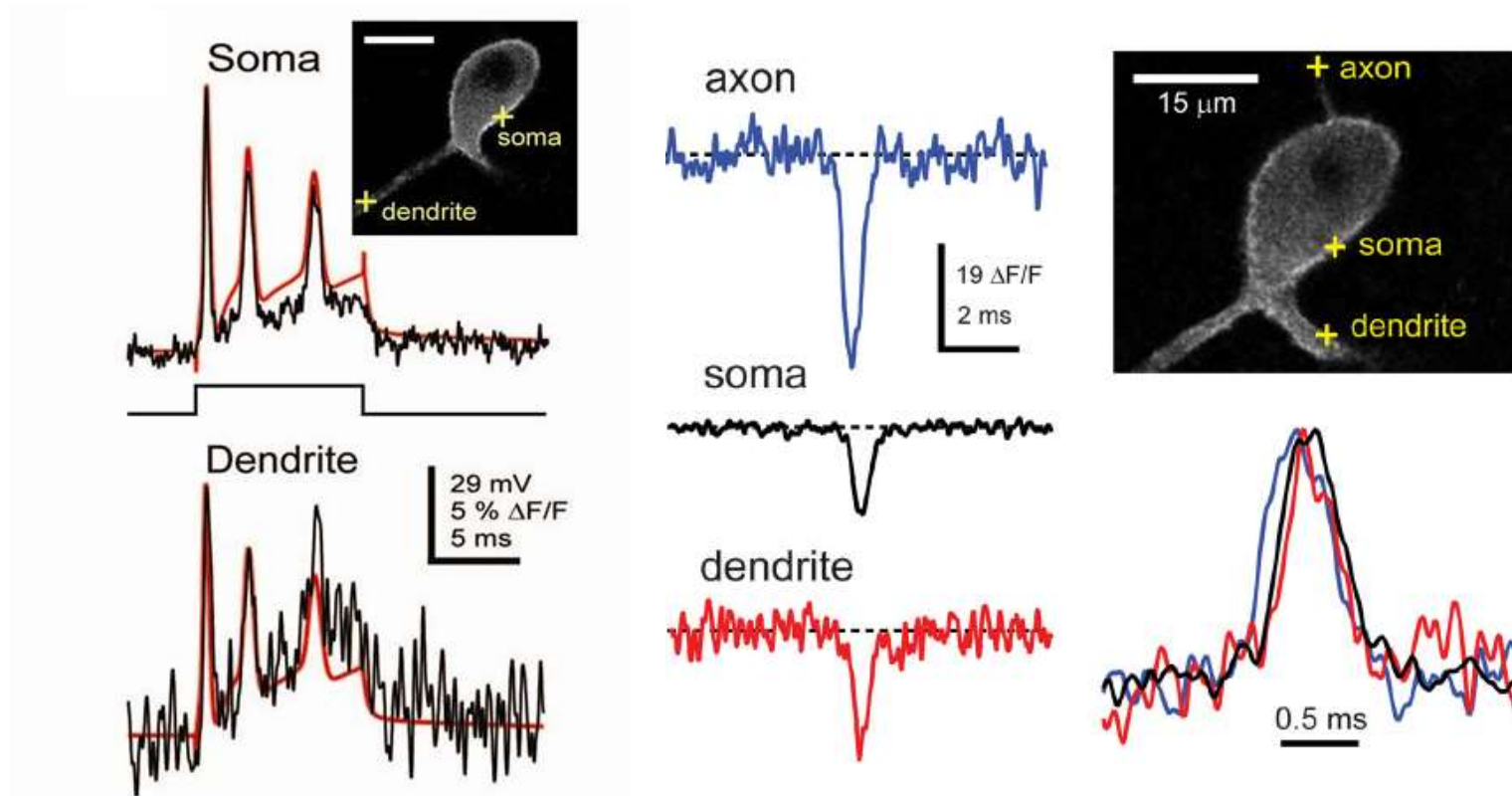
B



$\lambda = 940 \text{ nm}$
3 μM DPA

Fink et al., PLOS One, 2012

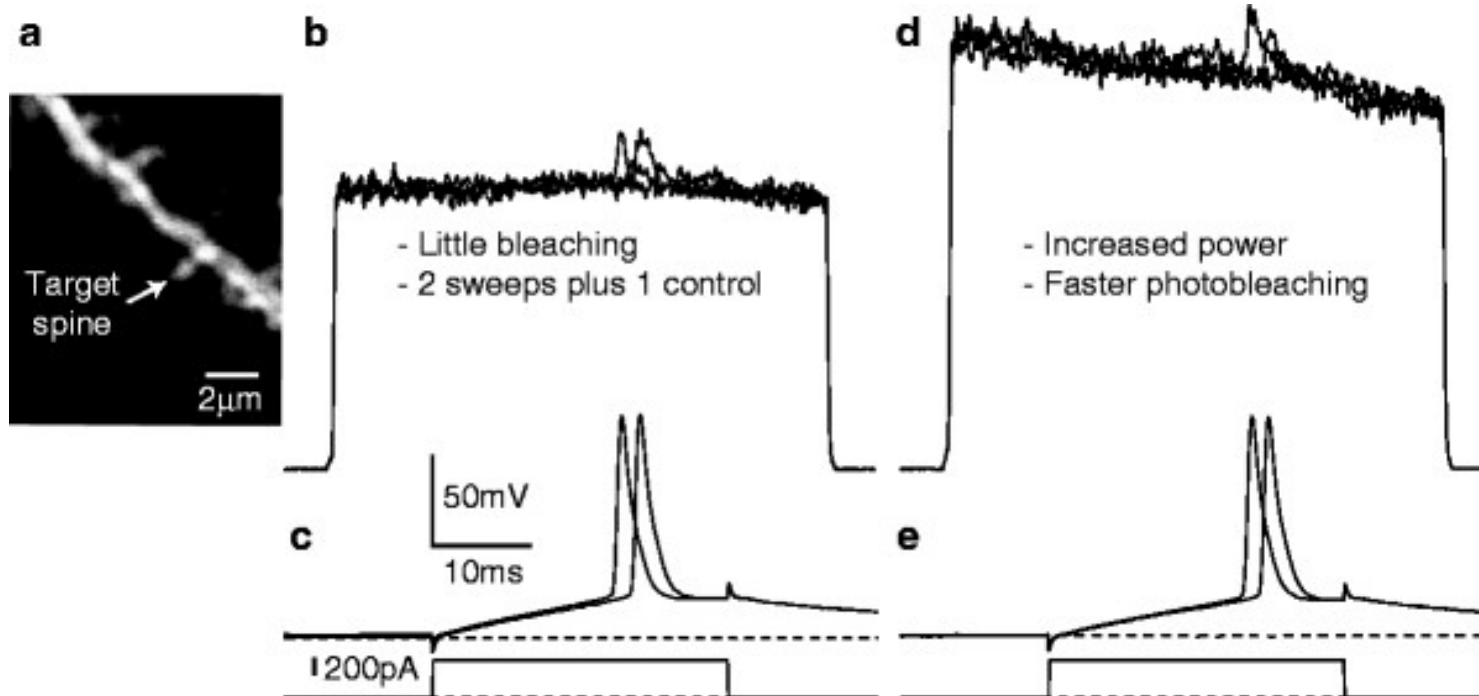
Laser spot photometry from different regions of the same neuron



Bradley et al., *J. Neurosci.*, 2009

Small molecule voltage dyes

JPW-3028



Acker & Loew, Ch. 11 *Chemical Neurobiology. Meth. Mol. Biol.*, 2013, doi.org/10.1007/978-1-62703-345-9_11

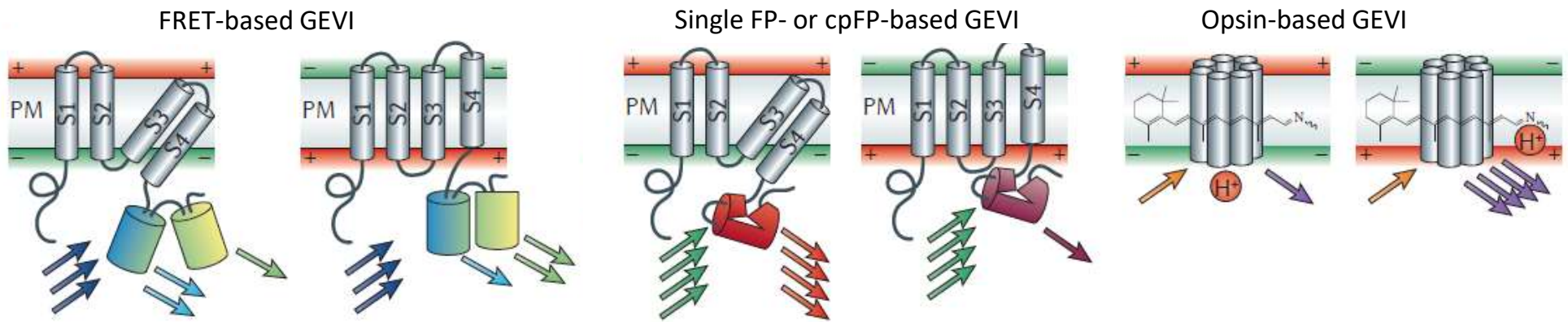
A comparison of genetic and non-genetic optical voltage sensors

Molecule	Approx $\Delta F/F$ per 100 mV	Approx response time	Comments
VSFP 2.3 ¹	9.5%	78 ms	Ratiometric ($\Delta R/R$)
VSFP 2.4 ¹	8.9%	72 ms	Ratiometric ($\Delta R/R$)
VSFP 3.1 ²	3%	1-20 ms	Protein
Mermaid ³	9.2%	76	Ratiometric ($\Delta R/R$)
SPARC ⁴	0.5%	0.8 ms	Protein
FlaSh ⁵	5.1%	2.8 – 85 ms	Protein
Flare ⁶	0.5%	10 – 100 ms	Protein
PROPS ⁷	150%	5 ms	Protein
di-4-ANEPPS ⁸	8%	< 1 ms	Dye
di-8-ANEPPS ⁹	10%	< 1 ms	Dye
RH237 ¹⁰	11%	< 1 ms	Dye
RH421 ¹¹	21%	< 1 ms	Dye
ANNINE-6plus ¹²	30%	< 1 ms	Dye
hVOS ¹³	34%	< 1 ms	hybrid
DiO/DPA ¹⁴	56%	< 1 ms	hybrid

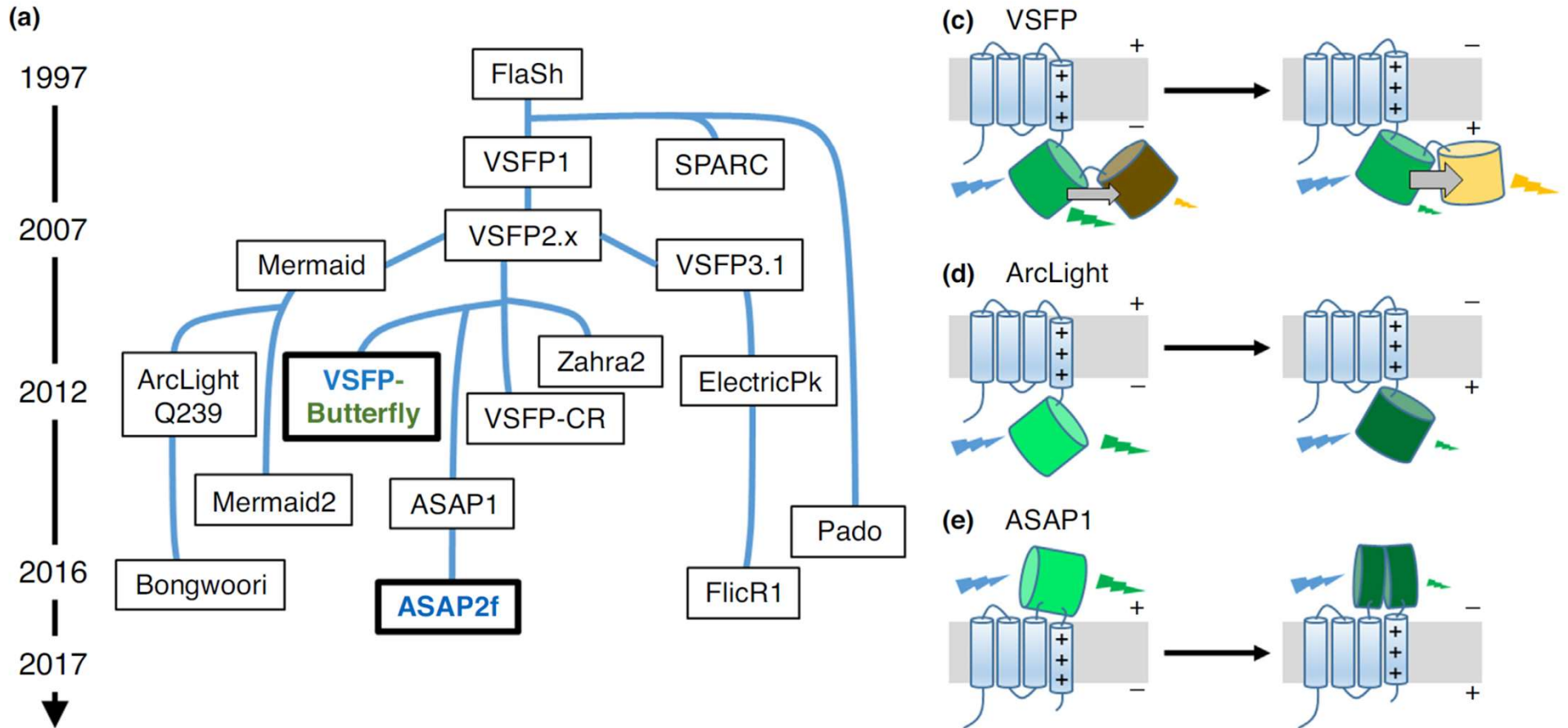
Supplementary Table 1 Approximate characteristics of fluorescent voltage indicating proteins. In some cases numbers were estimated from published plots. The table contains representative members of all families of fluorescent indicators but omits many.

from Supplementary Material Kralj et al., *Nat. Methods*, 9: 90-5, 2011; see also Table 1 in Xu et al, *Curr. Op. Chem. Biol.*, 2017

Genetically encoded voltage indicator (GEVI) strategies

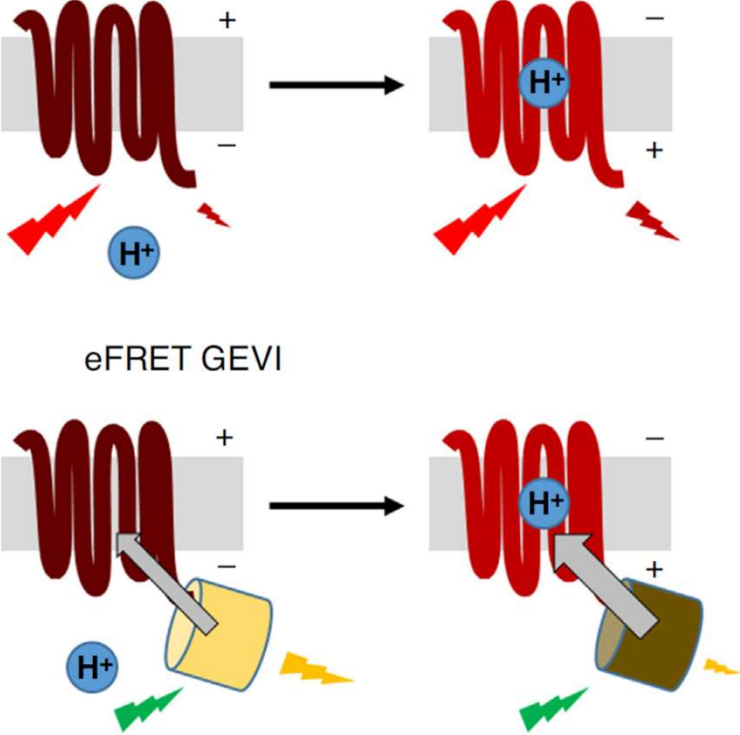
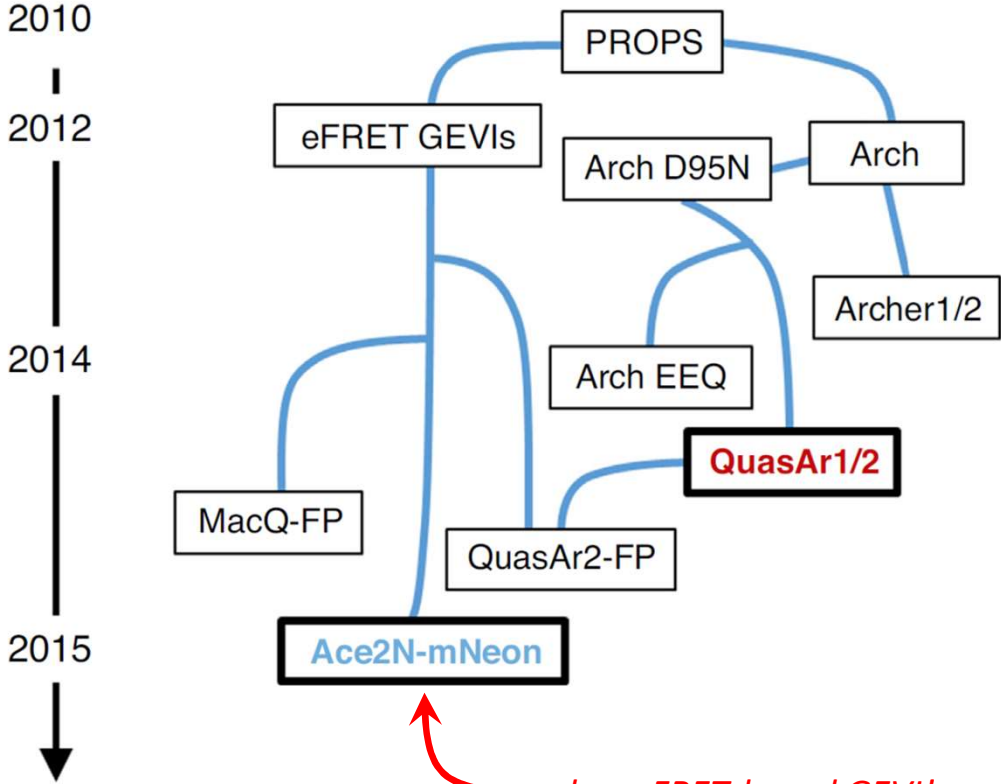


Circularly-permuted FP-based GEVIs



Xu et al. *Curr. Opin. Chem. Biol.* **39**: 1-10 (2017)

Opsin-based GEVIs



Current Opinion in Chemical Biology

Archaeorodopsin, an opsin-based GEVI

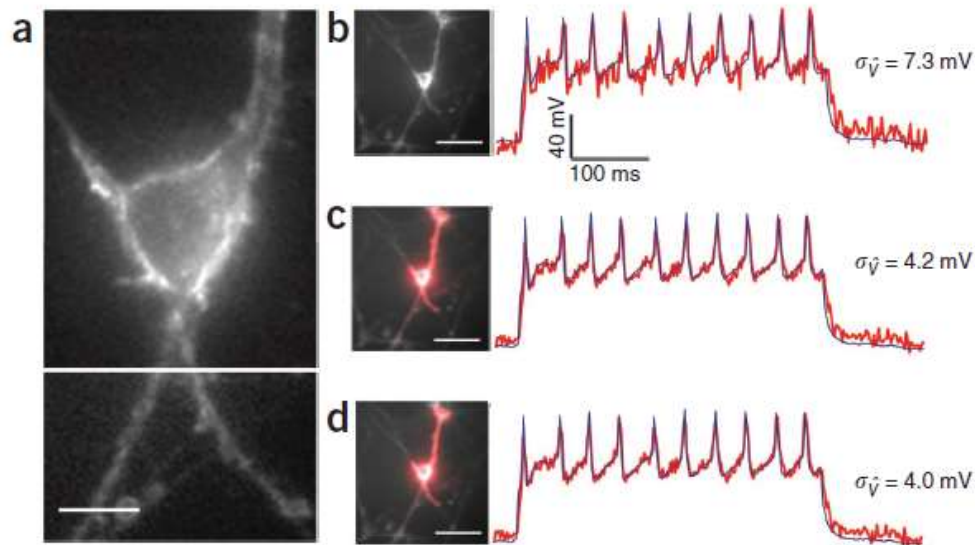


Table 1 | Optical and electrical response of Arch and Arch(D95N)

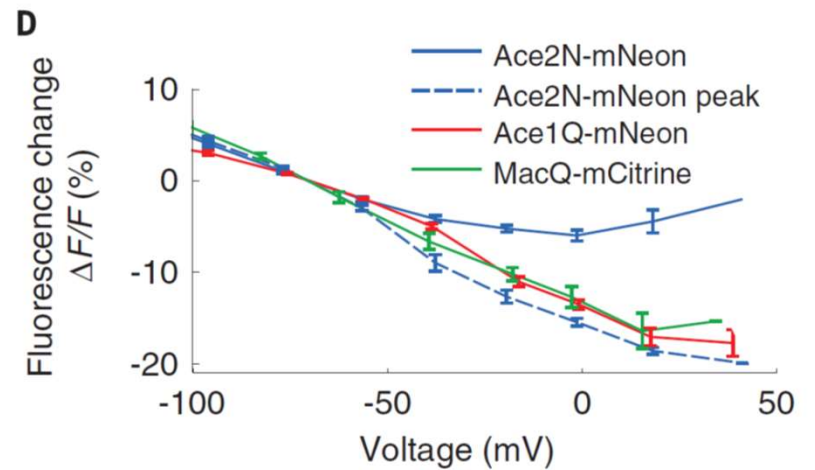
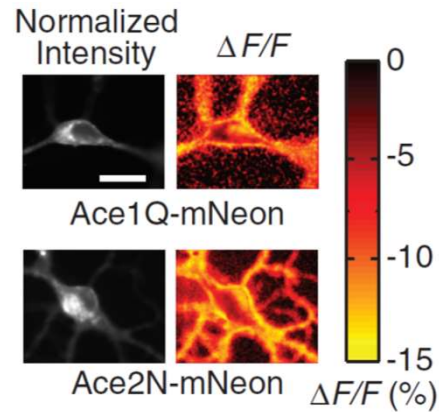
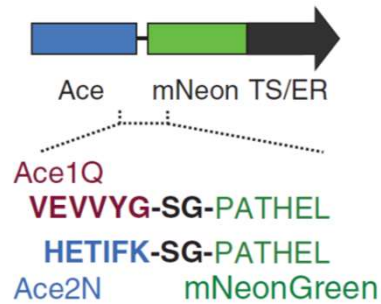
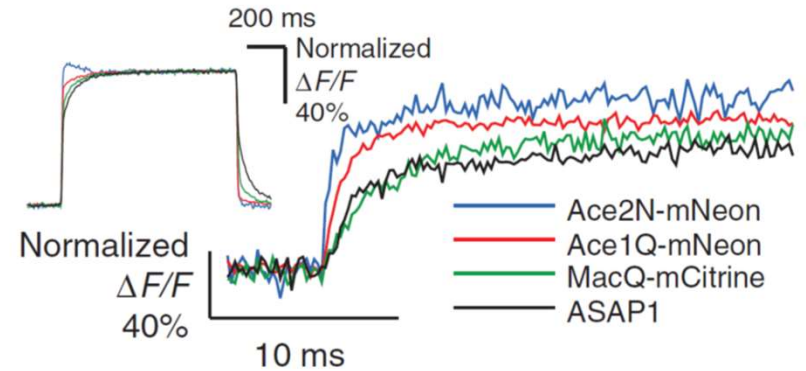
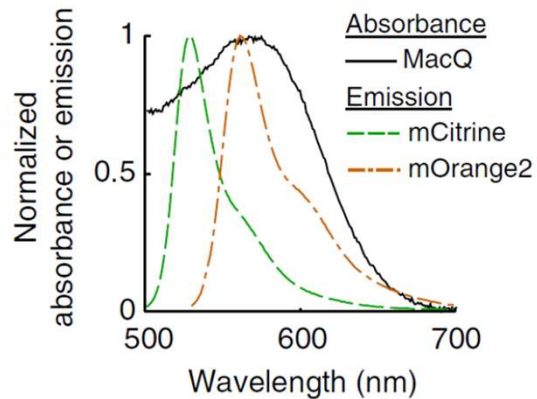
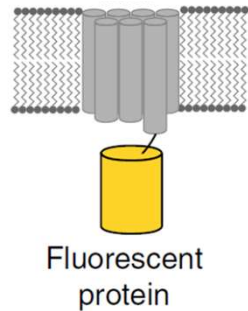
	λ_{\max} absorbance (nm)	λ_{\max} emission (nm) ^a	ϵ_{633} ($M^{-1} \text{ cm}^{-1}$) ^b	QY ^c	Photostability relative to eGFP ^d	pK _a of Schiff base ^e	τ_{response} (ms) ^f	Noise in \bar{V}_{FL} ($\mu\text{V Hz}^{-0.5}$) ^g	Photo-current
Arch	558	687	6,300	9×10^{-4}	0.25	10.1	<0.5	625	Yes
Arch(D95N)	585	687	37,500	4×10^{-4}	0.1	8.9	41	260	No

^c QY for eGFP is ~ 0.65 and for mNEON is ~ 0.8

Kralj et al., *Nat. Methods*, 9: 90-5, 2011

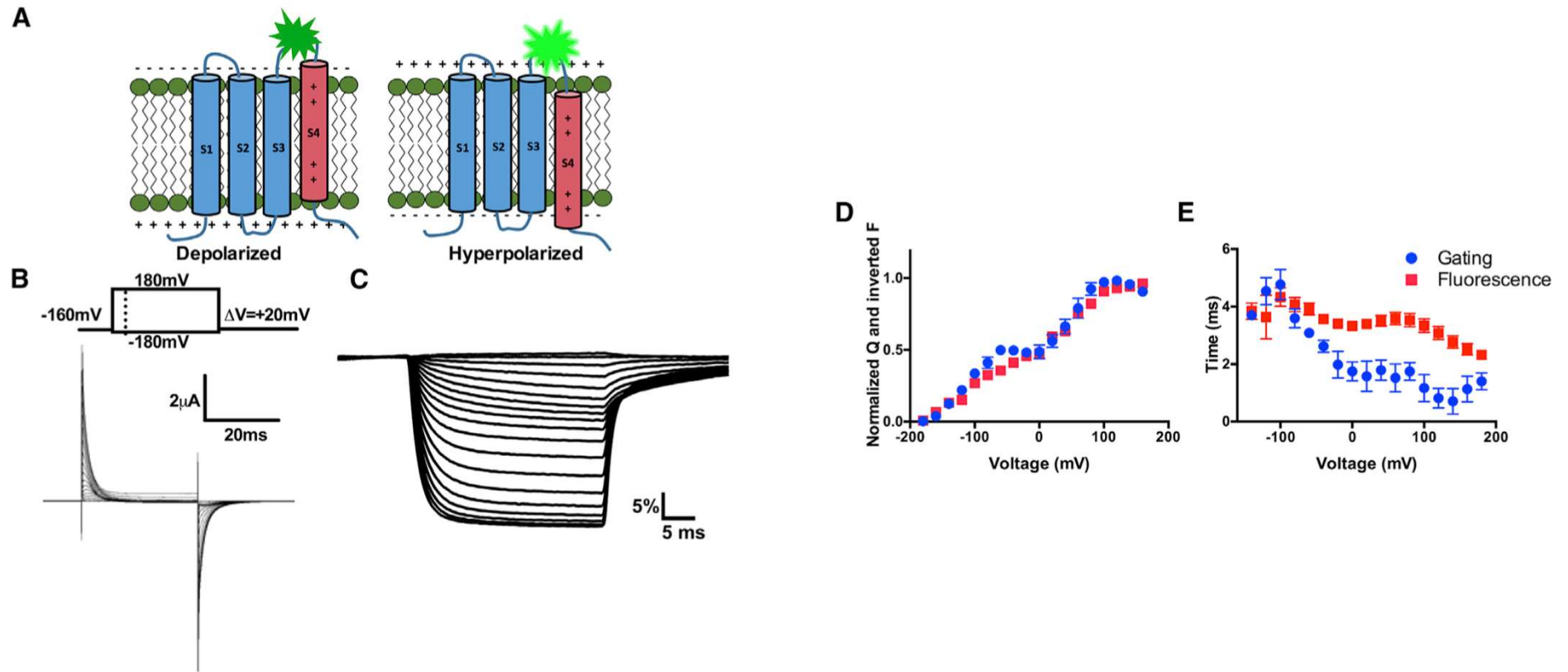
A FRET-based GEVI, *Ace2N-mNeon*

Opsin (McQ or Ace)



Gong et al., *Nat. Comm.* **5**: 3674, 2014; Gong et al., *Science*, **350**: 1361, 2015

The current state of the art- the cpGFP-based GEVI *ASAP1/2f*



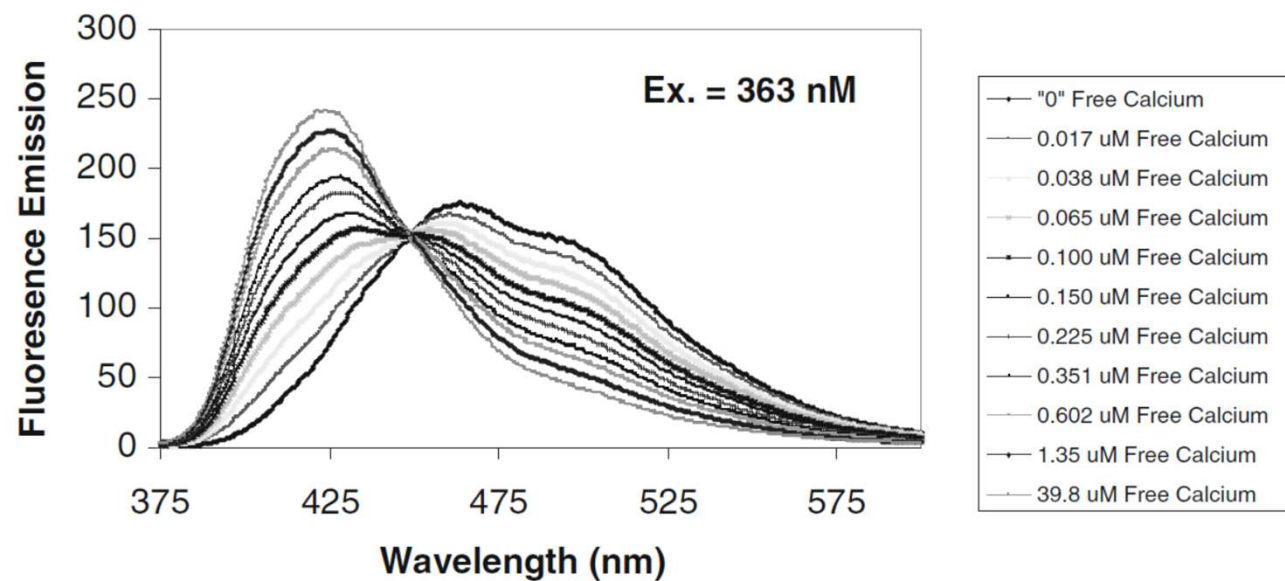
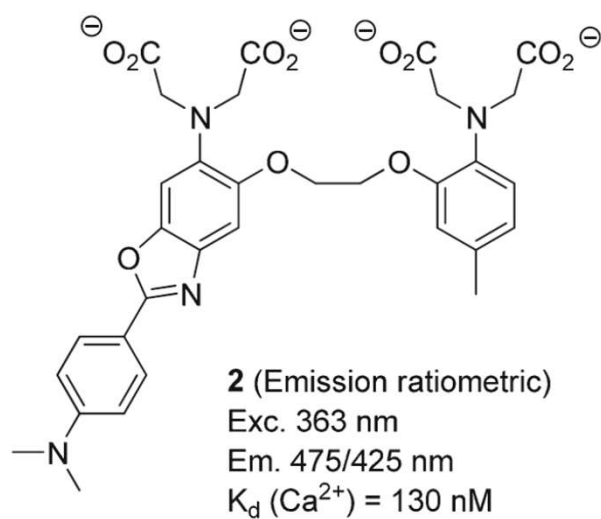
Why *in vivo* optical voltage measurements are challenging & GEVIs are not quite ready yet for recording single trial APs...

- Sensors have just become fast enough
- Sensors are not yet bright enough
- The brevity of AP signals makes measurement tough
(photon counts, instrumentation, etc.)
- Broad optical spectra (see FRET-based GEVIs) present challenges
- Sensors rely on charges in the membrane (=capacitive load)

Discussion: which approach best suits the experiment?



Ca⁺⁺ dye, ratiometric emission



Ca⁺⁺ dye, ratiometric excitation

